Chapter 5

CHAPTER-5

A CLASS OF SLIPLINE FIELD SOLUTIONS FOR METAL MACHINING WITH STICKING AND SLIPPING ZONES AT THE CHIP/TOOL INTERFACE WITH ELASTIC CONTACT

5.1 Introduction

A number of theoretical and experimental investigations have been carried out in the past to analyse the mechanics and to compute the interface stress distribution in metal machining. Such studies were initiated due to the fact that the stress distribution in the interface between the chip and the tool in the machining process affects the rate of wear and the life of cutting tool and determines its form-stability. Despite extensive research, there is still an inadequate understanding of the nature of distribution of stresses on the cutting tool during metal machining. The nature of variation of the interfacial stress distribution for the above process was first proposed by by Zorev[29]. According to him, the frictional stress must gradually increase following coulomb's law of friction from its minimum value at the chip releasing point till it attained its limiting value k (yield stress in shear of the work material) at some distance away from the tool tip. There after, its value must remain constant. Thus the natural contact length according to Zorev's hypothesis is assumed to consist of two distinct zones:- a zone of slipping

contact where the frictional stress is less than " k " and a zone of sticking contact where the frictional stress is equal to " k ".

Zorev's conjecture has been endorsed by Finnie and Shaw[17], Bhattacharya[32] from the qualitative examination of frozen chip samples and has been quantitatively verified by various investigators. Childs et al.[74], Barrow et al.[62], Kato et al.[48] and Buryta et al.[82] carried out split-tool technique to determine stress-distribution at the chip-tool interface. Photoelastic method has been used by various investigators like Andreev[20], Kattwinkel[19], Usui et al.[25], Rice et al.[38], Chandrasekharan et al.[33], Amini[42], Okushima et al.[46] and Bagchi et al.[70]. The visio-plasticity technique was adopted by Roth and Oxley[47], Roth[44] and Childs[52] in order to determine stress distribution at the chip-tool interface. These studies have established that the natural contact length consists of a zone of elastic contact where the stresses are below the yield limit and a zone of plastic contact where both slipping ($\tau \leq k$) and sticking regions ($\tau = k$) may be present.

In this chapter, slipline field solutions are presented for orthogonal machining process where the plastically deforming region may consist of both sticking and slipping zones. The fields analysed are those presented by Kudo[34] and discussed in the last chapter where their analysis was carried out by assuming the interface shear stress to be a constant proportion of yield stress k in shear ($\tau = mk$). In this section, the solution to the above fields are presented when coulomb friction obtains at the chip/tool interface. It is seen that at low values of friction coefficient μ, the solutions are governed by slipping friction only. Sticking regions in the plastic interface are predicted only when μ exceeds a

certain critical value. Under such conditions the above fields have to be modified in the manner discussed in the following sections. An elastic contact length with either a parabolic or an exponential normal stress distribution in this region is assumed to satisfy the statical requirements. Machining parameters and interface stress distributions are evaluated for both the fields for different tool geometries and cutting conditions. The extent of sticking and slipping zones in the natural contact length are evaluated and their variation with tool rake angle and interface friction coefficient μ is studied. The theoretically predicted results are found to agree reasonably well with experimental data reported in literature.

5.2 Slipline Fields

The two slipline fields under consideration are shown in Fig.5.1 and Fig.5.2 along with their associated hodographs.

Referring to Fig. 5.1(a), it may be seen that the curve ADC in this slipline model defines the primary shear line. The rigid -plastic boundary separating the chip from the plastically deforming region is indicated by ADE, where DE is the concave α -line and AD is the convex β - line. CDE is the plastically deforming material in contact with the tool. The angular range of slipline curves ED and DC are given by η and η_1 respectively. The angular range of these curves in this case are unequal as coulomb friction is assumed to apply on the tool face EC. The sliplines ED and DC meet the tool face at angles ϕ_E and ϕ_c ($\eta + \phi_E - \eta_1$) respectively.

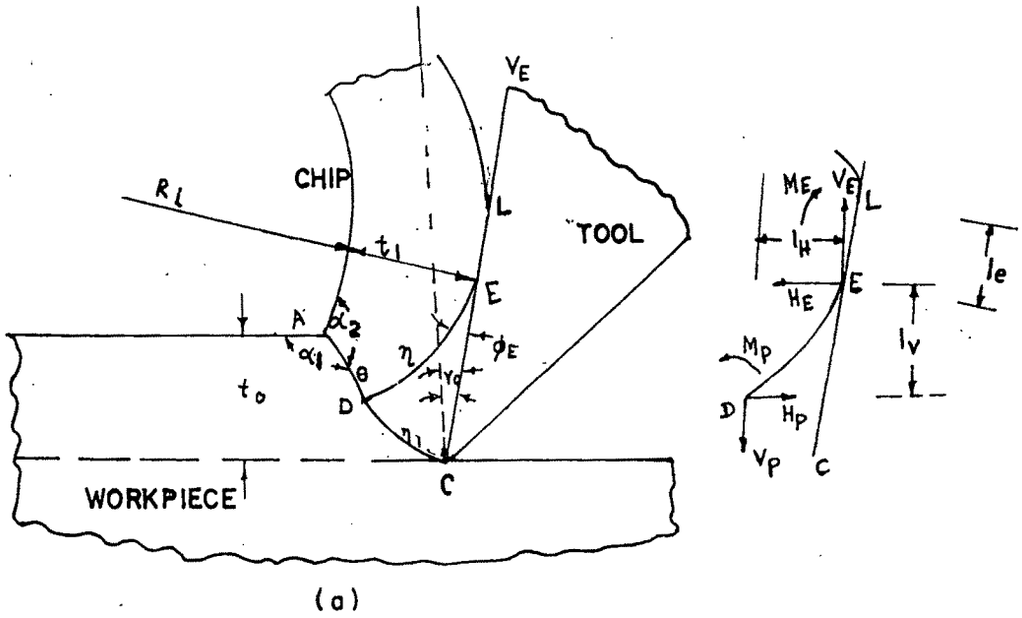

(a)

FIG. 5.1(a) SLIPLINE FIELD

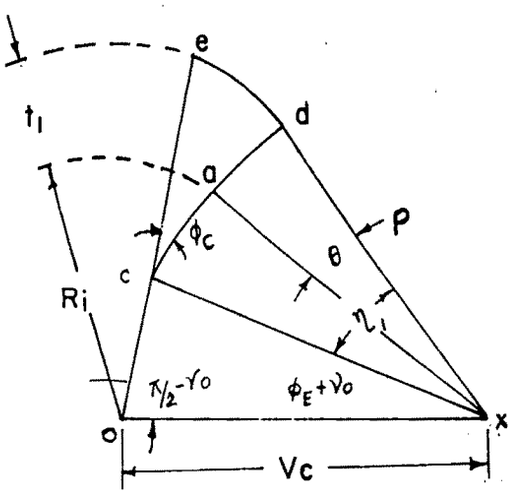

FIG. 5.1(b) HODOGRAPH

SOLUTION-I

Referring to the hodograph (Fig.5.1(b)) it may be observed that the material suffers a velocity discontinuity ρ on crossing the primary shearline. Thus, the velocity along the slipline ADC is given by the circular arc cd. Since the chip is rotating rigidly with the angular velocity ω, the curves ad and de in the hodograph are geometrically similar to the curves AD and DE in the slipline field respectively.

It may be mentioned that the angular range η of the slipline ED in Fig. 5.1(a) is less than$((1 / \mu + p_E - 2 \phi_E) / 4)$ (equation 3.1). This ensures that $\tau \leq k$ every where on EC and the chip/tool interface is governed by slipping friction only. The column vectors σ_{ED} and σ_{CD} representing the radii of curvature of the sliplines ED and CD respectively for this case are therefore calculated from the relations (refer to equation4.2)

$$\sigma_{ED} = (\rho/\omega) CL_{\phi_E \eta_1} \bar{c} \qquad (5.1)$$

and $$\sigma_{CD} = CL_{\phi_E \eta} \sigma_{ED} \qquad (5.2)$$

where, CL is the coulomb operator as discussed in [65][67].

For any given value of μ, when η reaches the limiting value given by equation (3.1), both sticking and slipping regions may be present in the chip/tool interface. Hence, the above slipline field has to be modified in the manner shown in Fig. 5.2 to take account of this boundary condition.

Referring to Fig 5.2 (a) it may be seen that the curve ABFG defines the primary shear line. The rigid - plastic boundary separating the chip from the plastically deforming region is indicated by ABDE, where BD and DE are the concave α - lines and AB is the convex β -line. CFG and CDE are the plastically deforming material in contact with the tool. GC is the zone of

sticking contact or the secondary shear zone($\tau = k$), where as CE is the slipping contact zone($\tau \leq k$). The angular range of slipline curves ED and DC are given by η and η_1 respectively in the slipping zone EDC. In the sticking zone, the angular range of slipline curves CF and FG are equal in magnitude ($= \psi$). It may be seen that the sliplines ED and DC meet the tool face at angles ϕ_E and $(\pi/2 - (\eta + \phi_E - \eta_1))$ respectively, where as the sliplines CF and FG meet the tool face at ϕ_c $(= \phi_E + \eta - \eta_1)$ and $(\pi / 2 - \phi_c)$.

Referring to the hodograph diagram (Fig. 5.2 (b)), it is made clear that the velocity along the slipline ABFG is given by the circular arc bg of radius ρ. Further the curves ab, bd and de are geometrically similar to their slipline images AB, BD and DE respectively. Hence slipline BA is also a circular arc of radius ρ.

Let σ_1, σ_2 and σ_3 denote the column vectors in the power-series expansion of the radius of curvature of the sliplines ED, BD and CD respectively. These are determined from their hodograph images as follows:

$$gb = - \rho \bar{c}$$

Hence, $cf = -G_{\phi_c \psi} \rho \bar{c}$

and $fc = -R_\psi G_{\phi_c \psi} \rho \bar{c}$.

The curves cd and db are determined from the circular arc fb and curve fc.

Thus, $cd = - P^*_\psi \rho \bar{c} - Q^*_\psi R_\psi G_{\phi_c \psi} \rho \bar{c}$

and $bd = -Q^*_{\eta_1} \rho \bar{c} - P^*_{\eta_1} R_\psi G_{\phi_c \psi} \rho \bar{c}$

Therefore, $ed = CL_{\phi_c \eta_1} cd$

But ed = $\omega \sigma_1$ and bd = $\omega \sigma_2$

Hence,

$$\sigma_1 = (-\rho/\omega) CL_{\phi_{\xi\eta}} [P^*_{\psi} + Q^*_{\psi} R_{\psi} G_{\phi_c \psi}] [\bar{c}] \quad (5.3)$$

$$\sigma_2 = (-\rho/\omega) [Q^*_{\eta} + P^*_{\eta} R_{\psi} G_{\phi_c \psi}] [\bar{c}] \quad (5.4)$$

and $\sigma_3 = CL_{\phi_{\xi\eta}} \sigma_1$ (5.5)

where CL is the coulomb operator[65], G is the straight rough boundary operator[55] and P*, Q* , R are standard matrix operators [49] and $\bar{c}$ is a column vector representing a unit circle.

The column vectors for the radii of curvature of other sliplines and hodograph curves are readily determined using the general matrix operator procedure developed by Dewhurst and Collins[49].

The second slipline field model involving sticking and slipping contact shown in Fig 5.3 (a) is very similar to that given in Fig 5.2 (a) except that a singular field ABD is now superimposed on the primary shearline AB. Referring to the hodograph (Fig. 5.3 (b)) it may be seen that gb is a circular arc of radius ρ. The column vectors for the radii of curvature of sliplines ED and AD are determined using coulomb operator [65] and matrix operators [49] from the circular arc gb.

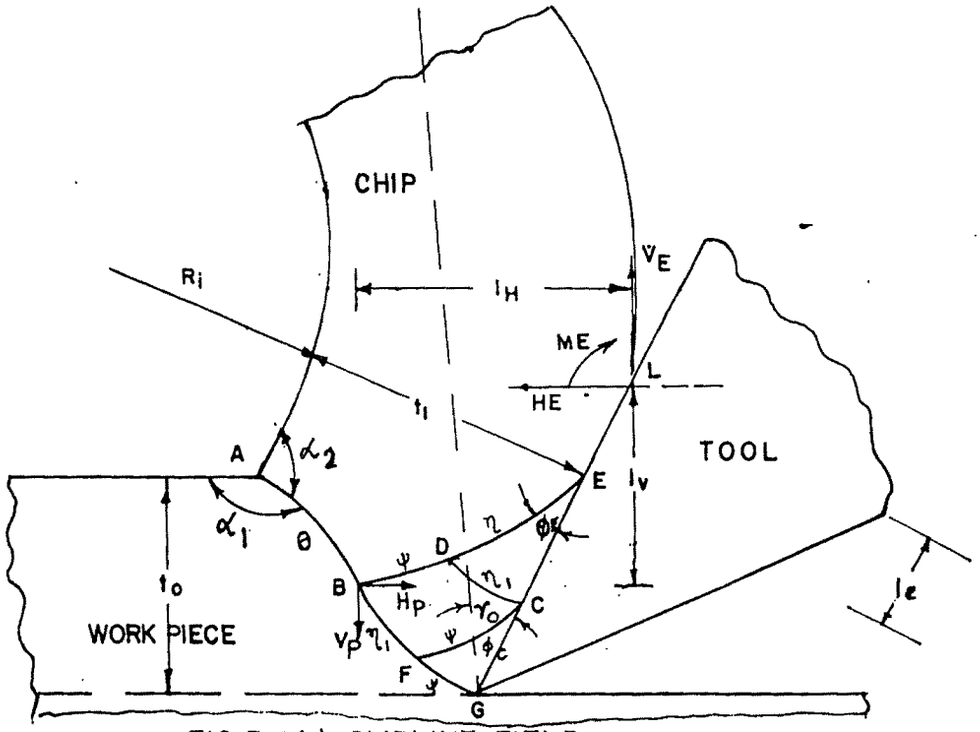

FIG. 5.2(a) SLIPLINE FIELD

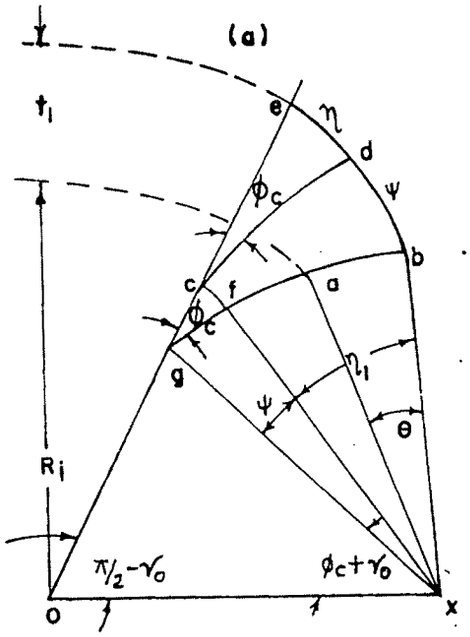

FIG. 5.2(b) HODOGRAPH

SOLUTION-II

Let σ'_1, σ'_2 and σ'_3 denote the column vectors in the power series expansion of the radius of curvature of sliplines ED, DA and DC respectively (Fig.5.3(a)).

Referring to Fig.5.3(b), we have $gb = -\rho\,\bar{c}$

Hence, $fc = -R_\psi G_{\phi_c\psi}\,\rho\,\bar{c}$

Also,

$cd = -P^*_\psi \rho\bar{c} - Q^*_\psi R_\psi G_{\phi_c\psi}\,\rho\,\bar{c}$

$ad = S_\alpha\, cd = -S_\alpha (P^*_\psi\rho\bar{c} + Q^*_\psi R_\psi G_{\phi_c\psi}\,\rho\,\bar{c})$ where, $\alpha = \eta_1 - \theta$

$bd = -P^*_{\eta_1} R_\psi G_{\phi_c\psi}\,\rho\bar{c} - Q_{\eta_1}\rho\,\bar{c}$

$ed = CL_{\phi_E\eta_1} cd = \omega\,\sigma'_1$

$da = -R_\theta S_\alpha (P^*_\psi + Q^*_\psi R_\psi G_{\phi_c\psi})\rho\,\bar{c} = \omega\, DA$

Thus,

$DA = (-\rho / \omega) R_\theta S_\alpha (P^*_\psi + Q^*_\psi R_\psi G_{\phi_c\psi})\,\bar{c}$

Hence,

$$\sigma'_1 = (-\rho/\omega) CL_{\phi_c\eta} [P^*_\psi + Q^*_\psi R_\psi G_{\phi_c\psi}][\bar{c}] \qquad (5.6)$$

$$\sigma'_2 = (-\rho/\omega) R_\theta S_\alpha (P^*_\psi + Q^*_\psi R_\psi G_{\phi_c\psi})[\bar{c}] \qquad (5.7)$$

and $$\sigma'_3 = CL_{\phi_E\eta}\sigma'_1 \qquad (5.8)$$

5.3 Methodology

The slipline fields presented in Fig.5.1, Fig.5.2 and Fig 5.3 were analysed using the same procedure as outlined in sections 3.2 and 3.3.

The non-linear relation between the angular ranges η and η_1 of the α- and β-lines respectively in the slipping zone EDC was approximated by the linear relation, $\eta_1 = B_0 \eta$. The linear coefficient B_0 was then calculated by solution to the transcedental equations(3.28) and (3.25) and the linear regression equation(3.29). The value of B_0 so obtained was now used to evaluate the coulomb operator CL. The slipline fields were then constructed using the operator CL and the standard matrix operators by solution to equations 5.1 - 5.8. The accuracy in these cases was also of the same order as that for the slipline fields discussed in chapter III ($\mu = 0.6$, $\tau = 0.98k$ and $\mu = 0.8$, $\tau = 0.99k$ in the sticking zone CFG).

It may be noticed that in these fields, the chip boundary is defined by three field variables. These are: the angular range θ of the β - line, angular range η / ψ of the α lines and the hydrostatic pressure P_E at E (In Fig 5.2(a) and Fig 5.2(b), $\eta = ((1/\mu) - p_E - 2\phi_E)/4)$. The static equilibrium of the chip was realised by imposing externally the forces and moment on the chip in the elastic contact region as discussed in section 4.3. For any given pressure distribution in the elastic contact length, the elastic contact forces H_E, V_E and elastic moment M_E are readily calculated. For equilibrium of the chip, these together with the forces H_P, V_P and

moment M_P calculated from the slipline curves in the chip boundary must simultaneously be equal to zero. Mathematically this condition may be stated as:

$$F_1 = H_P - H_E = 0 \qquad 5.11(a)$$

$$F_2 = V_P - V_E = 0 \qquad 5.11(b)$$

$$F_3 = M_P - M_E + H_E L_H + V_E L_V = 0 \qquad 5.11(c)$$

A FORTRAN programme developed for analysing the above fields calculated the forces H_P, V_P and moment M_p in the chip-boundary using the subroutines given in[49]. For any given value of η / ψ and pressure distribution in the elastic contact zone (parabolic or exponential), the programmes then solved the above set of non-linear algebraic equations with the help of an algorithm developed by Powell [51]. Static equilibrium was assumed to be achieved when the values of θ, P_E and X (ratio of the elastic to the plastic contact length) computed in the above manner satisfied the inequality:

$$F_1^2 + F^2_2 + F^2_3 \leq 10^{-10} \qquad (5.12)$$

The programme then used the values of the optimised field variables to compute the machining parameters such as uncut chip-thickness, cutting ratio, curl radius, cutting and thrust forces, total contact length, sticking-contact length etc. It also contained checks to determine whether rigid vertices at A were overstressed [15]. The range of permissible values of p_A for which valid solutions are obtained, is governed by equation(3.32). The volume constancy condition was found to be satisfied . The programme also incorporated flatness and traction checks as discussed in section 3.3. All

programmes were run on a ALPHA DEC SERVER and the time required for each calculation was less than one second.

5.4 Results and discussion

The permissible ranges of the machining parameters as a function of the angular range η of the base slipline ED(Fig. 5.1) are presented in Fig. 5.4 for a cutting tool with 10^0 rake angle for solution I. In this case parabolic normal stress distribution was assumed in the elastic contact length with a constant coefficient of friction $\mu = 0.4$ at the chip/tool interface. Referring to the above figure it may be seen that the lower limiting value of η in this case is zero. Under this condition solution I reduces to the slipline field proposed by Lee and Shaffer. The elastic contact lengths (l_e / t_0) for this case for $\eta = 0$ is also found to be zero as is proved in Appendix A. Angle η attains its upper limiting value(η_{UL}), when the vertex angle α_1 at A is overstressed. For all rake angles studied, the permissible solution range was found to lie within these two limits.

It may be seen with reference to Fig. 5.4 that the cutting force (F_c / kt_0), the thrust force (F_t / kt_0) and cutting ratio (t_1 / t_0) are maximum when $\eta = 0$ and their values decrease as η increases. The natural contact length (l_t / t_0), the elastic contact length(l_e / t_0) and the radius of chip-curl (t_0 / R_m), on the other hand, attain their minimum values when $\eta = 0$ and these are found to increase as η increases. Similar trend was observed for all tool rake angles γ within the limits $0 \leq \gamma \leq 15^0$ (refer to Fig. 4.3 and Fig. 4.4, chapter 4).

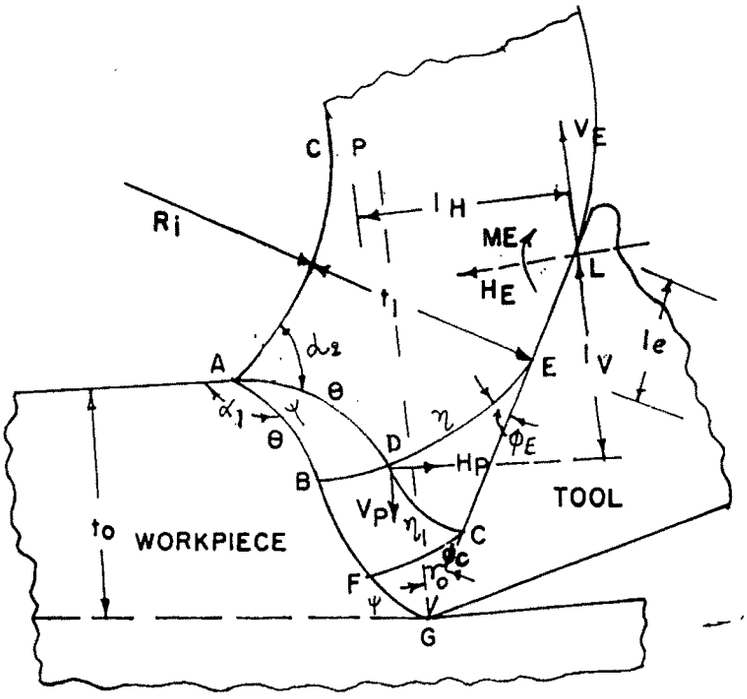

FIG.5.3(a) · SLIPLINE FIELD

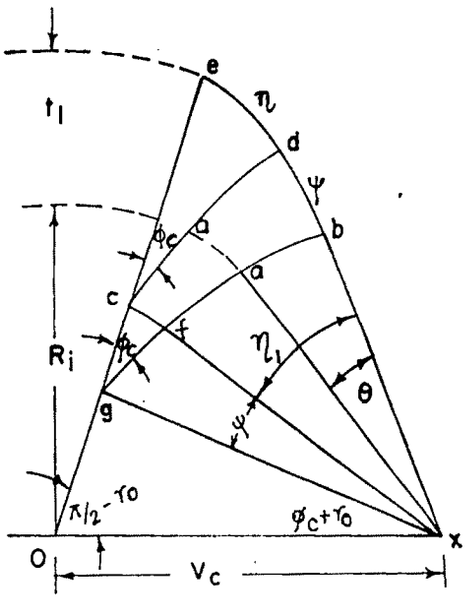

FIG.5.3(b) HODOGRAPH

SOLUTION-III

The variation of machining parameters with field angle ψ (angular range of sliplines in the sticking zone) as computed from solution II (Fig.5.2) and solution III (Fig. 5.3) are presented in Fig. 5.5 and Fig. 5.7 for a tool with zero degree rake angle and in Fig5.6 and Fig. 5.8 for a tool with 15^0 rake angle respectively. In all cases a parabolic normal stress distribution was assumed in the elastic zone with a constant coefficient of friction of $\mu = 0.7$ at the chip/tool interface.

Referring to the above figures it may be seen that the minimum value of ψ in all these cases is zero. Under this condition, solution II and solution III reduce to solution I (Fig.5.1). The sticking length (l_s / t_0) for these cases for $\psi = 0$ is also zero. The upper limiting value of ψ (ψ_{UL}) in all these cases is attained when the vertex angle α_1 at A is overstressed. For all rake angles studied, the permissible solution range was found to lie within these two limits ($\psi = 0$ and $\psi = \psi_{UL}$).

It may be seen with reference to Fig.5.5 that for solution II the cutting force ($F_c / k\, t_0$), the thrust force ($F_t / k\, t_0$), the cutting ratio (t_1 / t_0) and the natural contact length (l_t / t_0) are maximum when $\psi = 0$ and their values decrease as ψ increases. The elastic contact length (l_e / t_0), the sticking length(l_s / t_0) and the radius of chipcurl (t_0 / R_m), on the other hand, attain their minimum values when $\psi = 0$ and these are found to increase as ψ increases. The natural contact length in Fig 5.6 for solution II increases as ψ increases but other parameters follow the same trend. Similar trend of variation of machining parameters is also observed for solution III (Fig. 5.7 and Fig. 5.8). However, values of

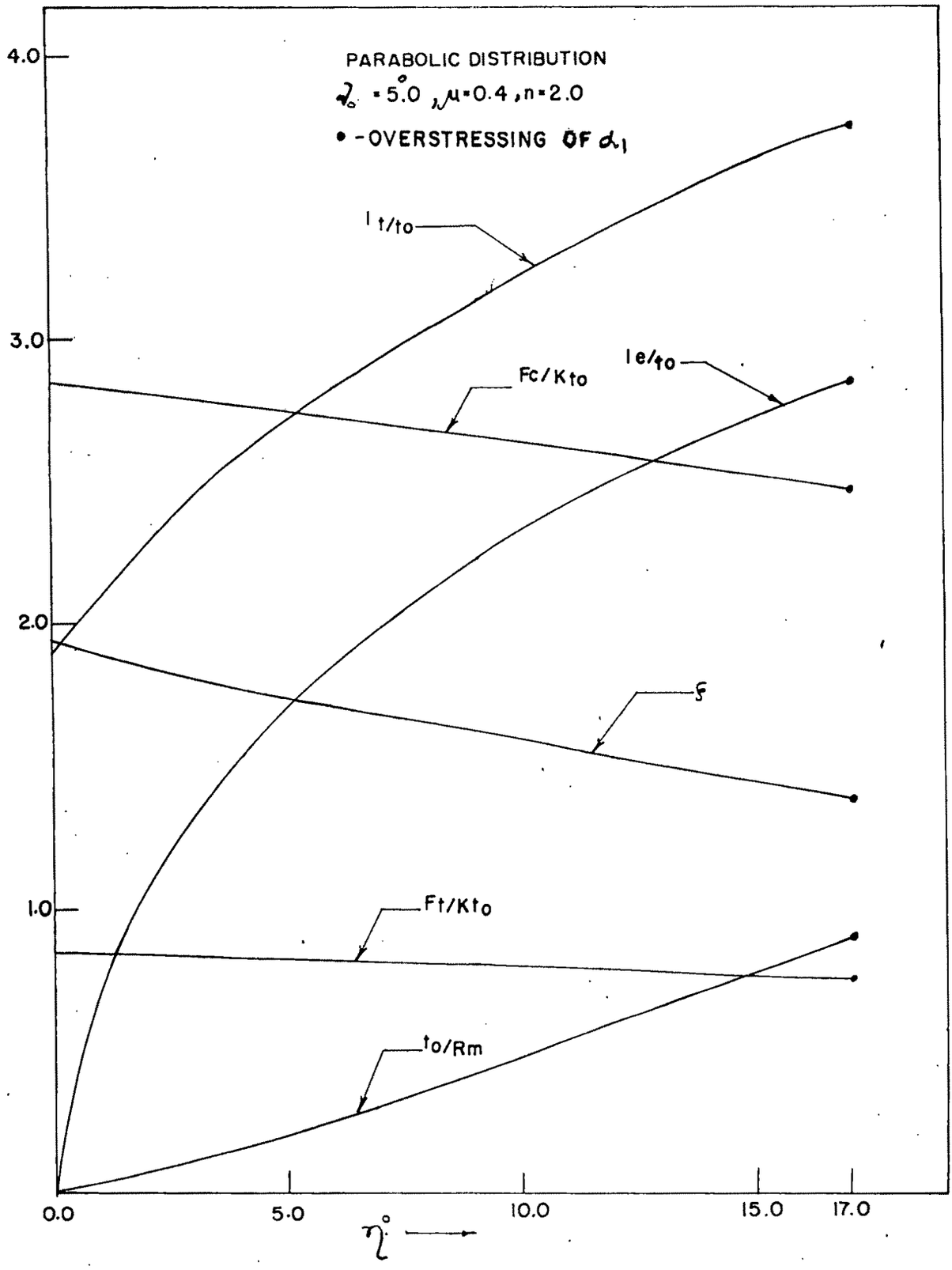

FIG. 5.4 VARIATION OF MACHINING PARAMETERS WITH η FOR SOLUTION-I (FIG. 5.1)

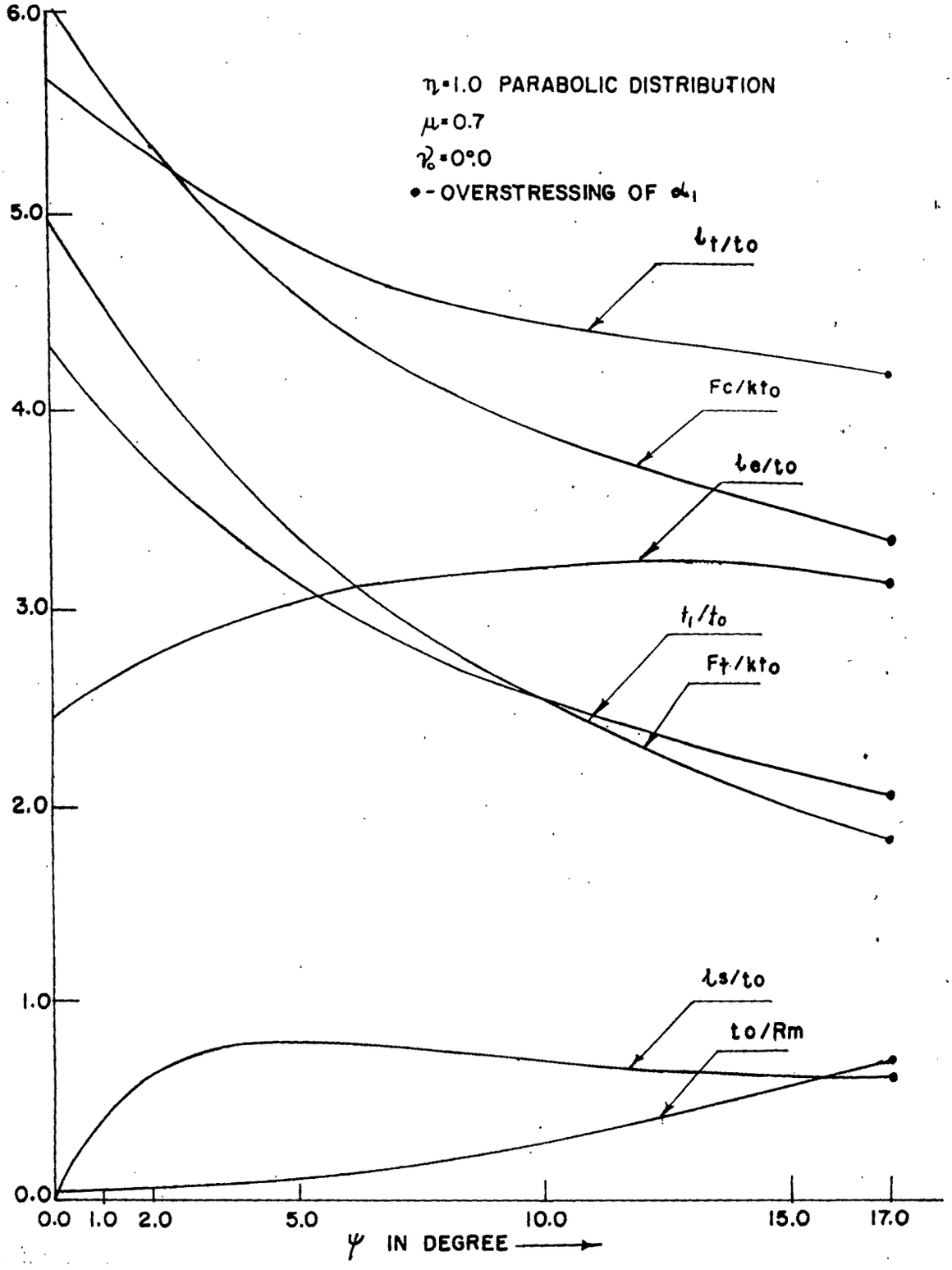

FIG. 5.5 VARIATION OF MACHINING PARAMETERS WITH ψ FOR SOLUTION -II (FIG. 5.2)

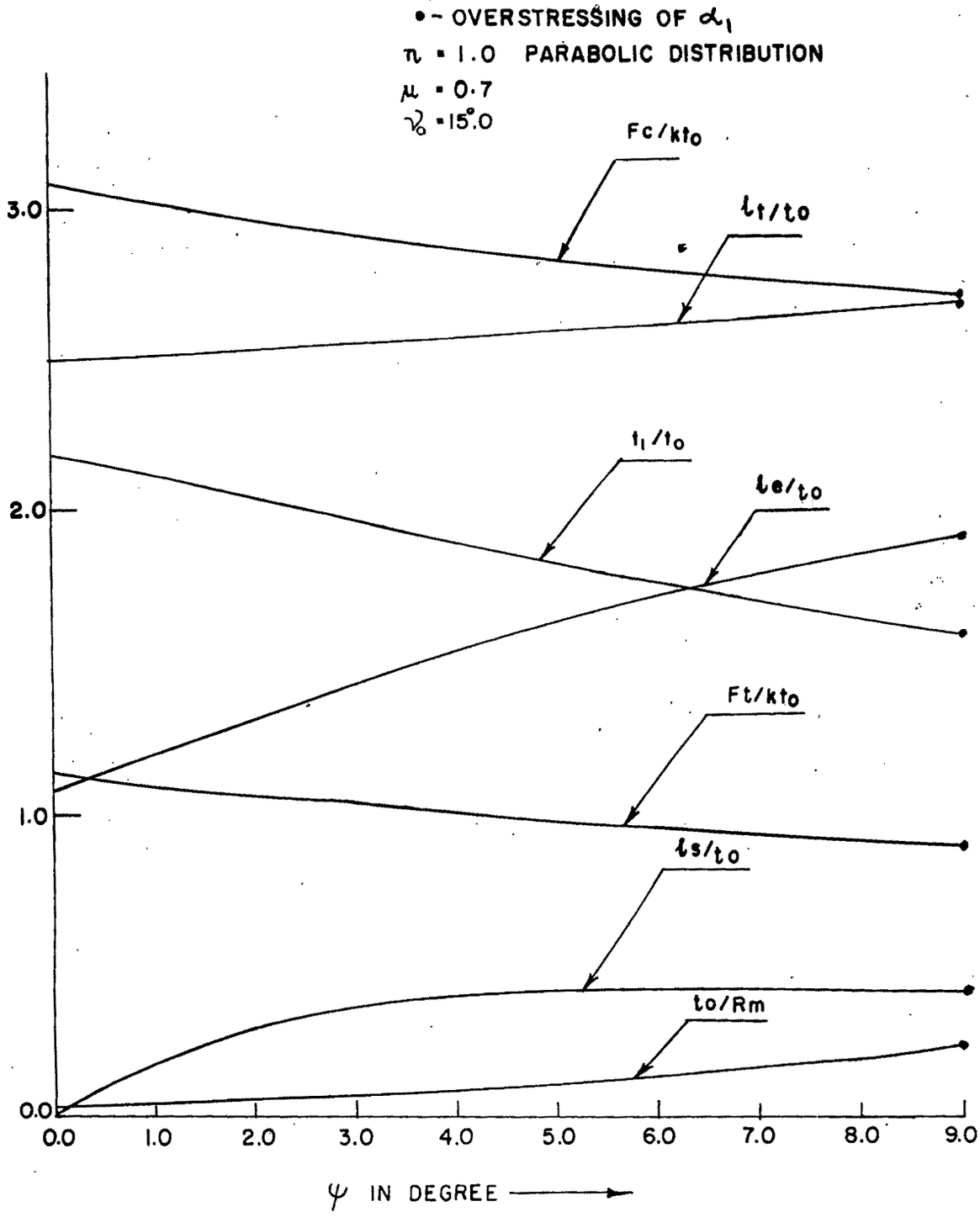

FIG. 5.6 VARIATION OF MACHINING PARAMETERS WITH ψ FOR SOLUTION-II (FIG. 5.2)

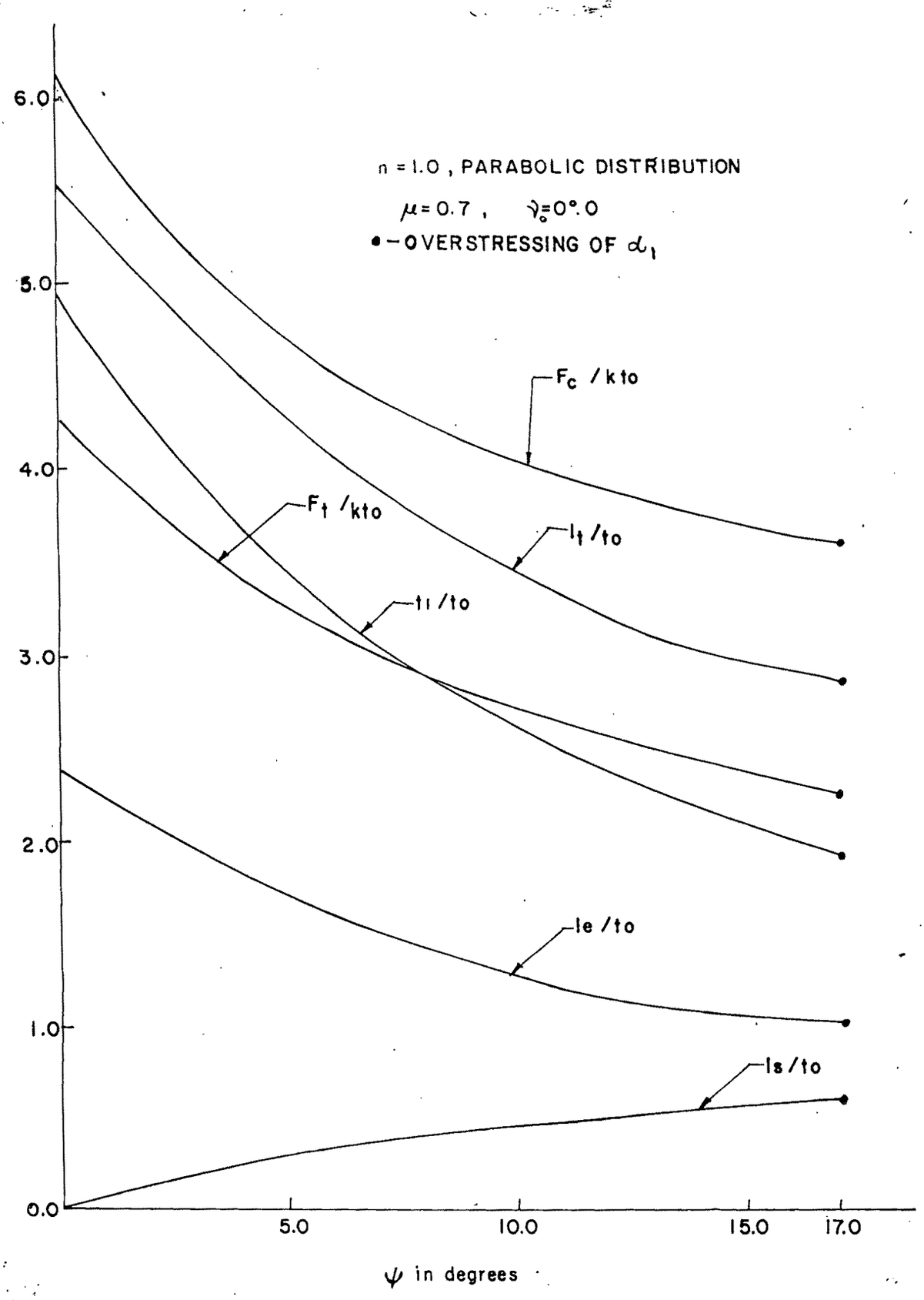

FIG.5.7 VARIATION OF MACHINING PARAMETERS WITH ψ FOR SOLUTION – III (FIG.5.3)

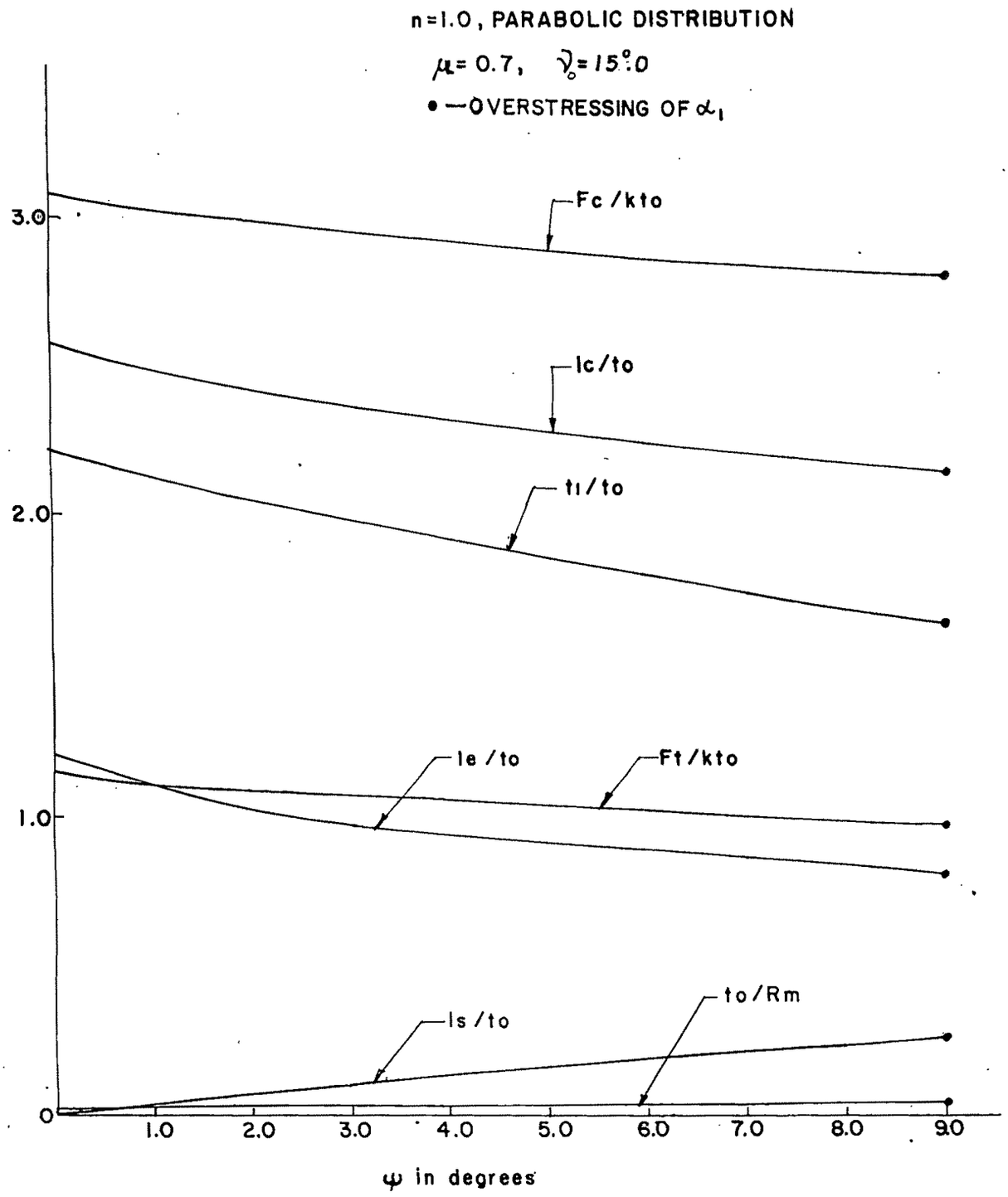

FIG. 5.8 VARIATION OF MACHINING PARAMETERS WITH ψ FOR SOLUTION-III (FIG. 5.3)

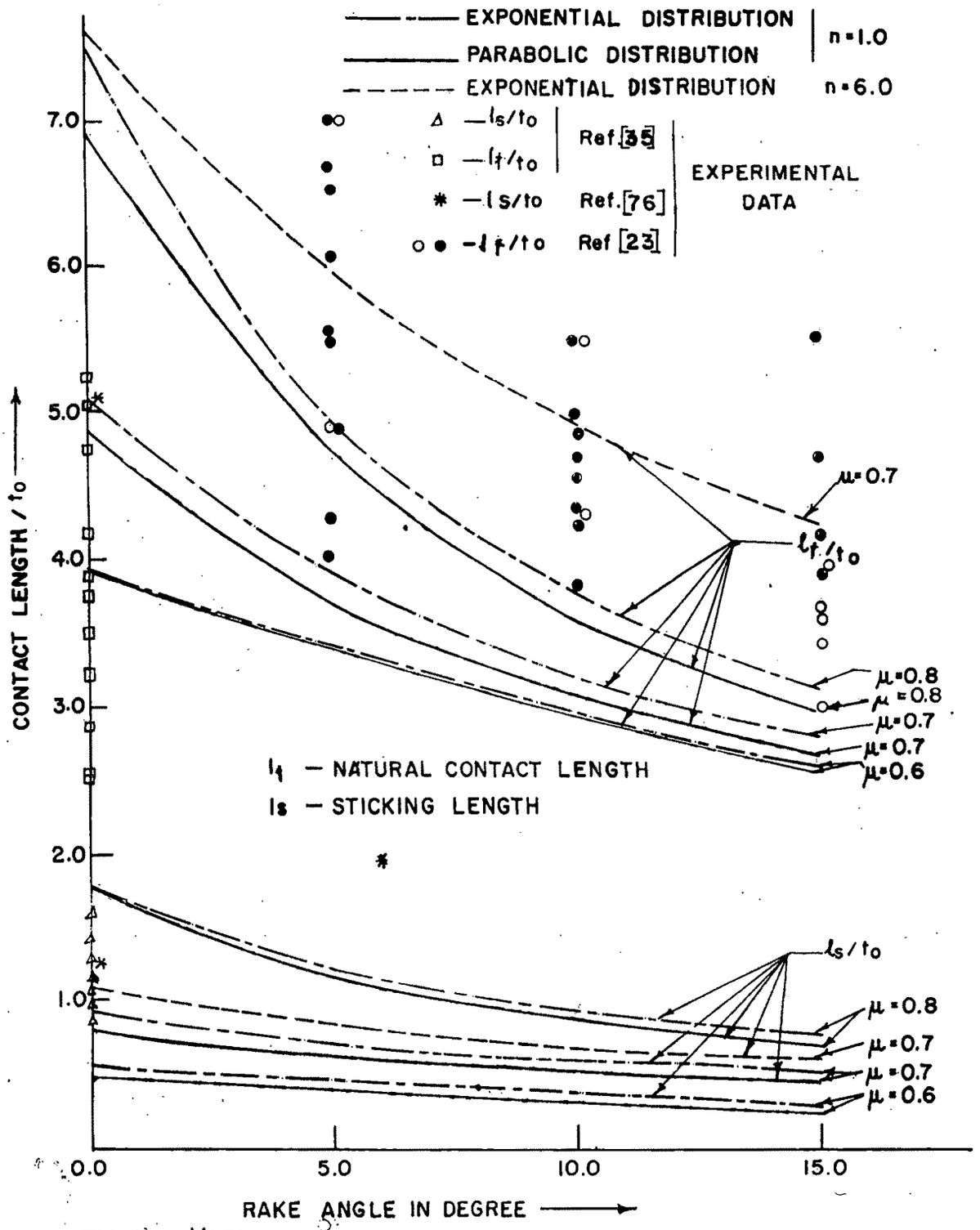

FIG.5.9 VARIATION CONTACT LENGTH WITH TOOL RAKE ANGLE GAMA (SOLUTION-II, FIG. 5.2)

natural contact length (l_t / t_0) and elastic contact length (l_e / t_0) decrease as ψ increases.

The variation of the natural contact length (l_t / t_0) and the length of sticking contact (l_s / t_0) with variation in tool rake angle as computed from solution II (Fig. 5.2) and solution III (Fig. 5.3) are presented in Fig. 5.9 and Fig. 5.10 respectively for different values of friction coefficient μ at the chip/tool interface. For a given friction condition and a given stress distribution in the elastic zone, the non-dimensionalised lengths reported in the above figures refer to their limiting values as calculated from overstressing consideration. Referring to the above figures it may be seen that the natural contact length (l_t / t_0) and the length of sticking contact (l_s / t_0) decrease with increase in tool rake angle and are found to increase with increase in the value of μ. The theoretical values are also found to agree reasonably well with the experimental results reported by Barrow et al.[62] and Childs et al[74], [76]. It is further observed that for solution III (Fig. 5.3) the sticking length (l_s / t_0) is almost independent of the nature of stress distribution in the elastic contact length (parabolic / exponential), though the natural contact length depends on the above stress distribution(Fig. 5.11). The sticking ratio (l_s / l_t) and the ratio of plastic contact length to length of natural contact (l_p / l_t) are also found to be nearly independent of the tool rake angle as is indicated by Fig. 5.12.

The variation of the normal and the shear stresses along the chip/tool contact length for the two solutions involving both sticking and slipping zones in the region of plastic contact (Fig. 5.2 and Fig. 5.3) are presented in Fig. 5.13 - Fig. 5.18 for a tool with zero degree rake angles. Results are given both for parabolic and exponential

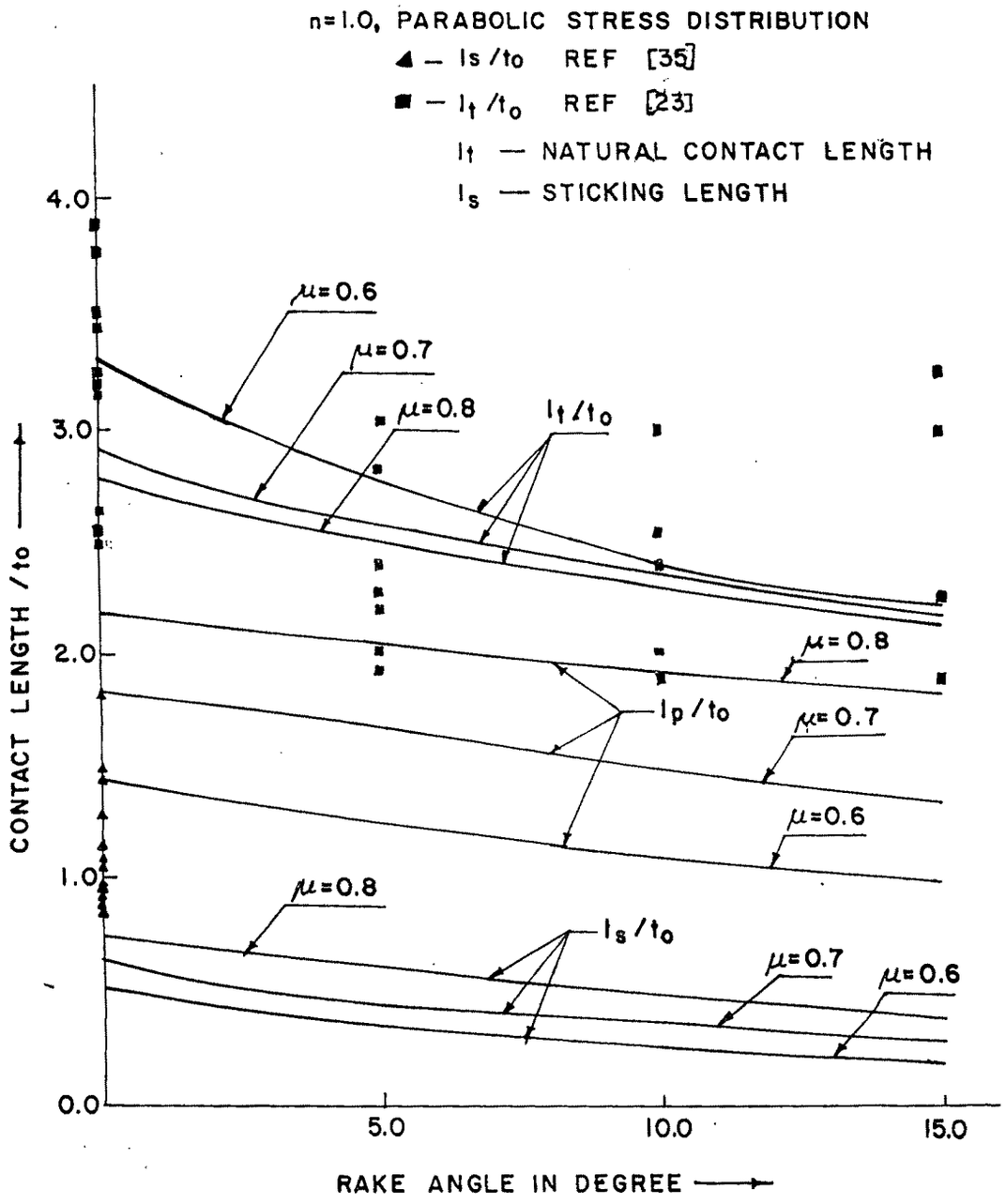

FIG.5.10 VARIATION OF CONTACT LENGTH WITH TOOL RAKE ANGLE (SOLUTION-III, FIG.5.3)

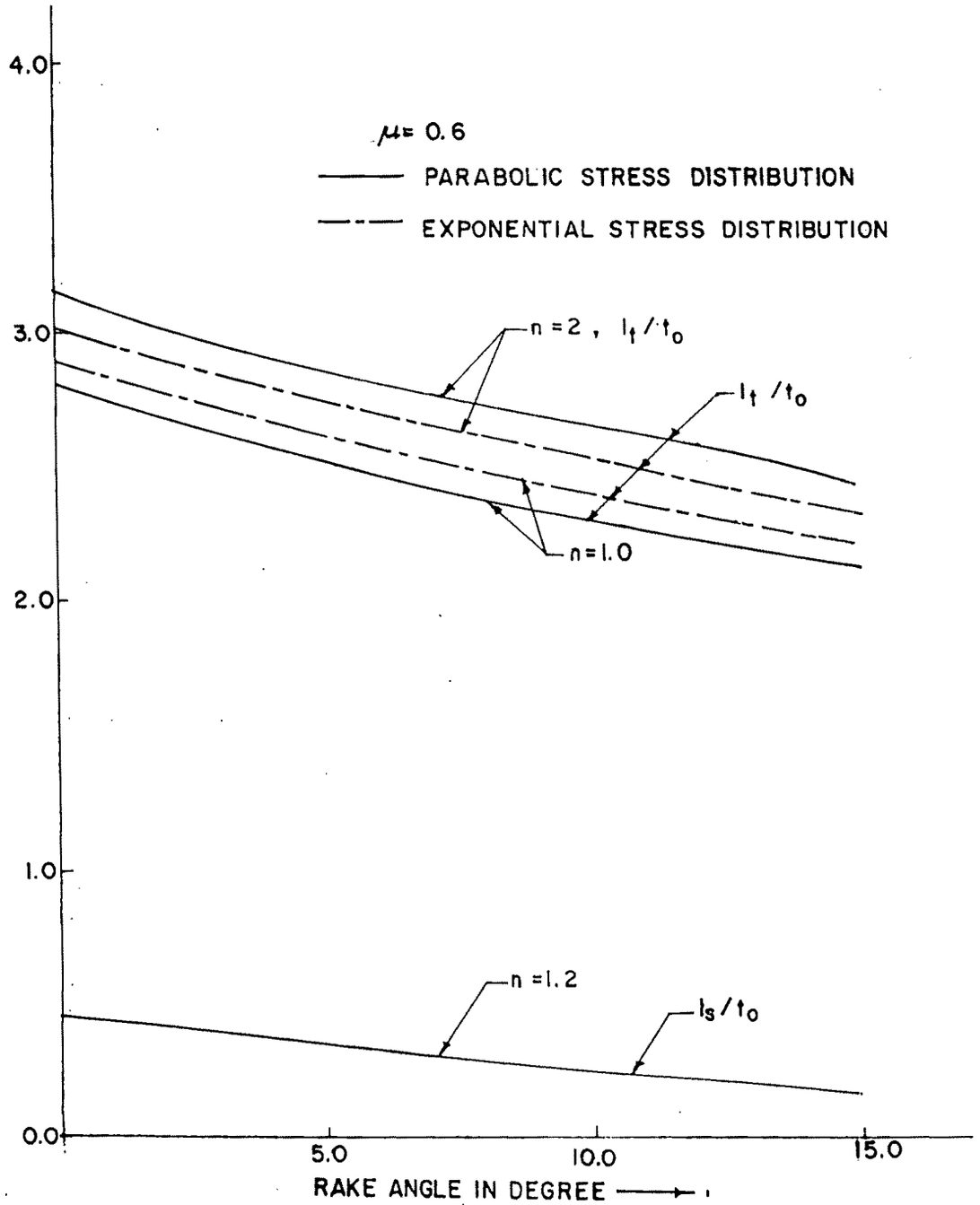

FIG. 5.11 DEPENDENCE OF CONTACT LENGTH ON NATURE OF STRESS DISTRIBUTION IN THE ELASTIC ZONE (SOLUTION-III)

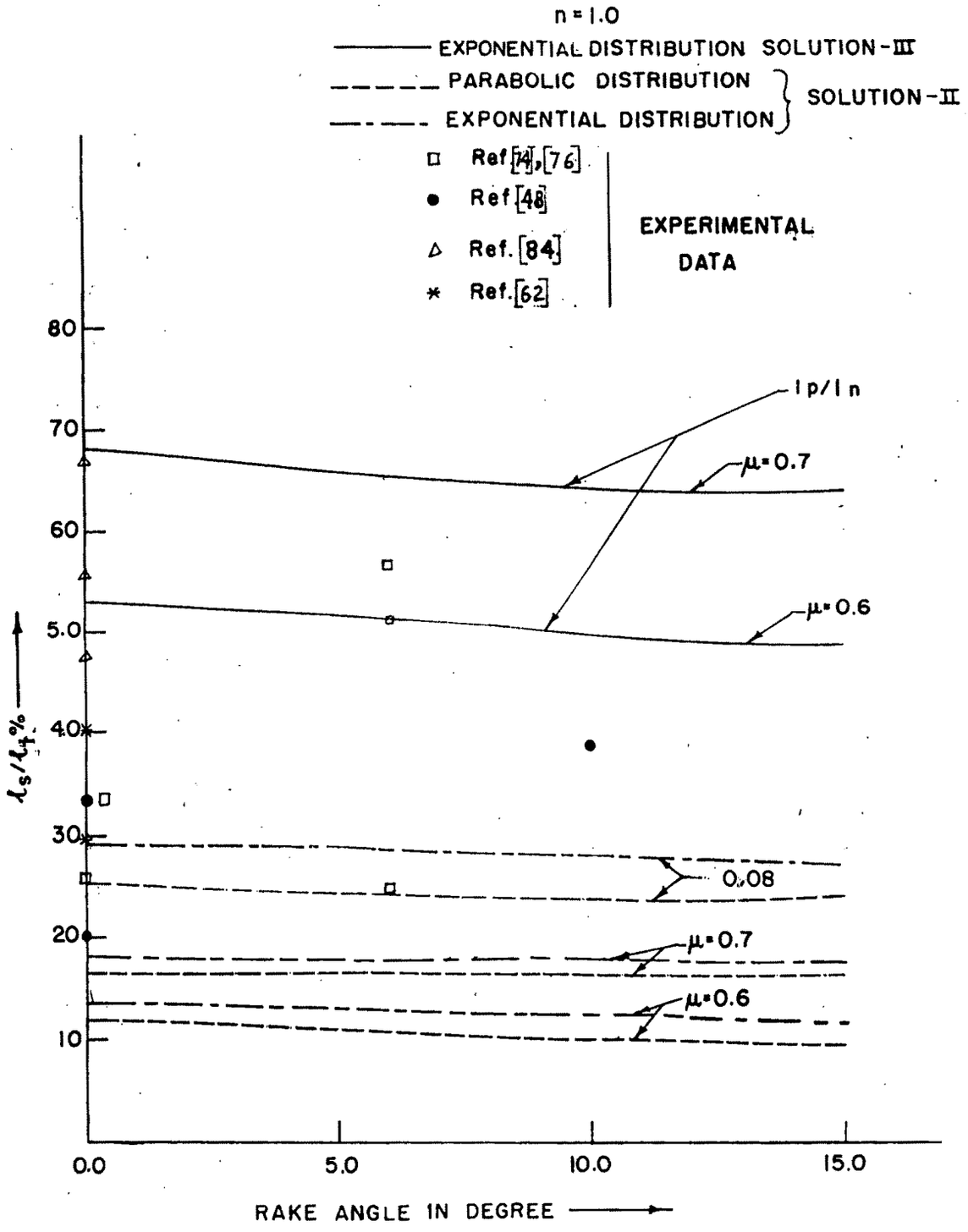

FIG.5.12 VARIATION OF STICKING RATIO AND PLASTIC CONTACT RATIO WITH RAKE ANGLE GAMA (SOLUTION II & III)

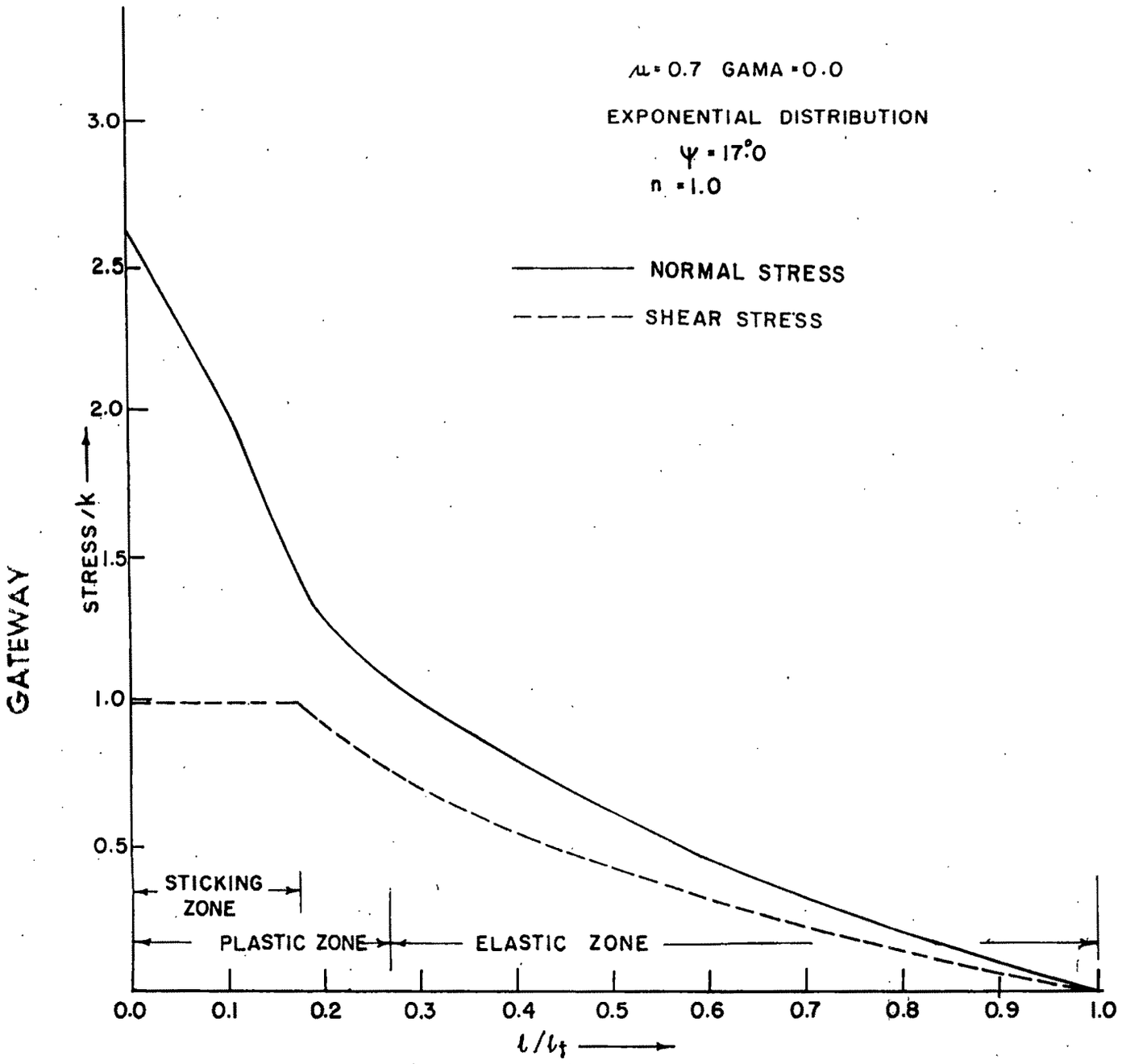

FIG.5.13 VARIATION OF INTERFACE CONTACT STRESS (SOLUTION-II FIG.5.2)

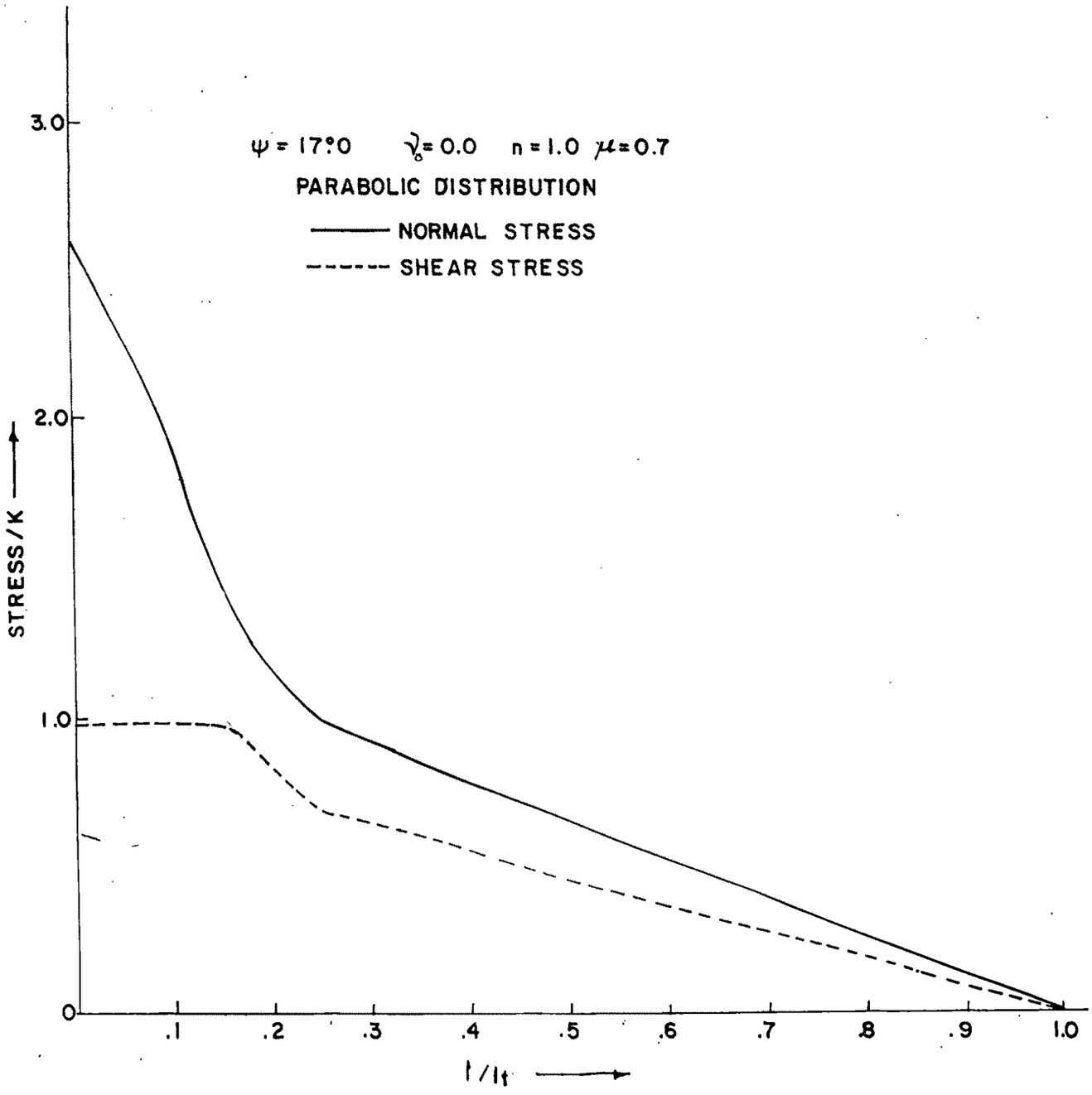

FIG. 5.14 VARIATION OF INTERFACE CONTACT STRESS (SOLUTION-II FIG.5.2)

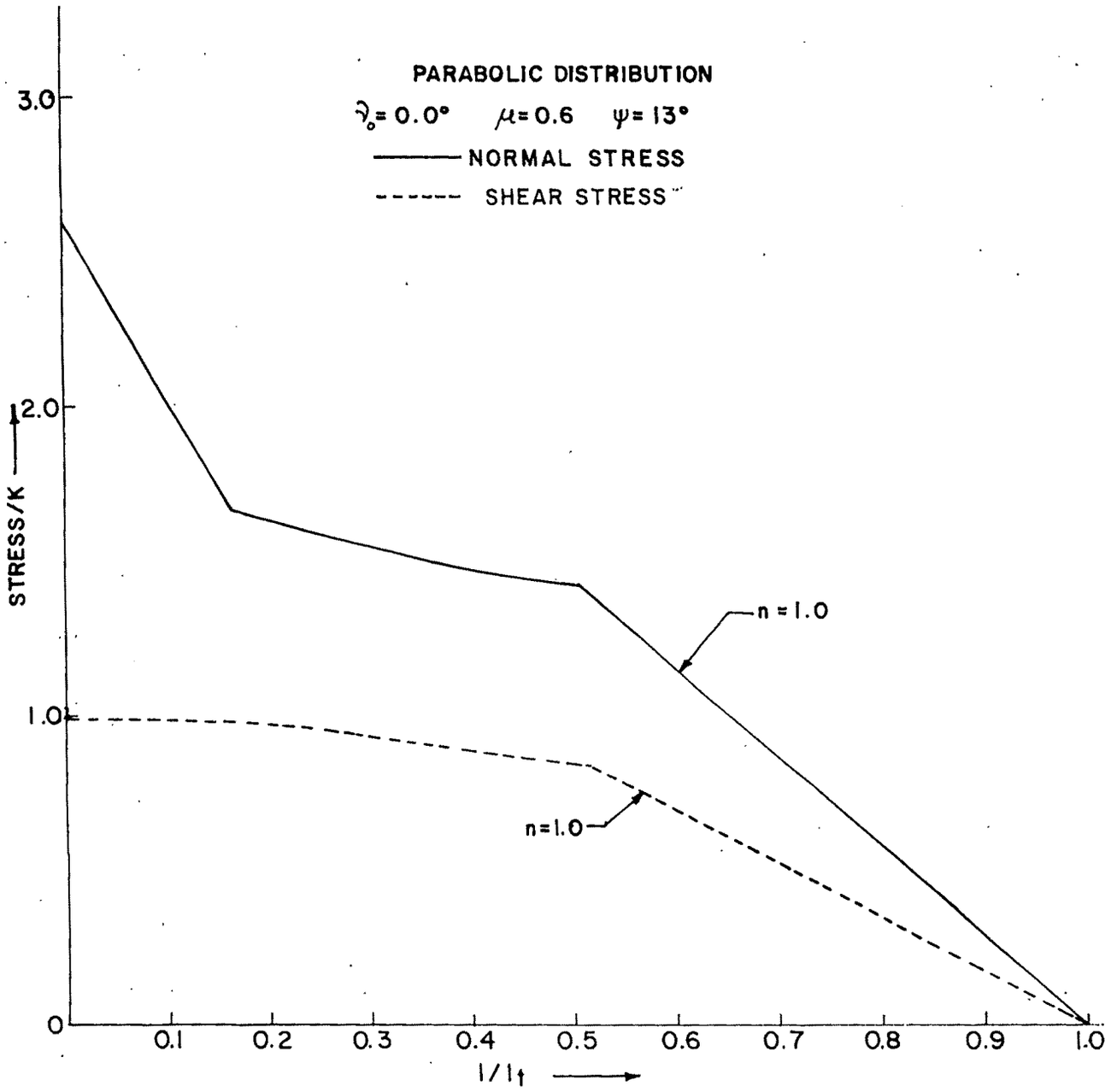

FIG. 5.15 VARIATION OF INTERFACE CONTACT STRESS (SOLUTION-III FIG. 5.3)

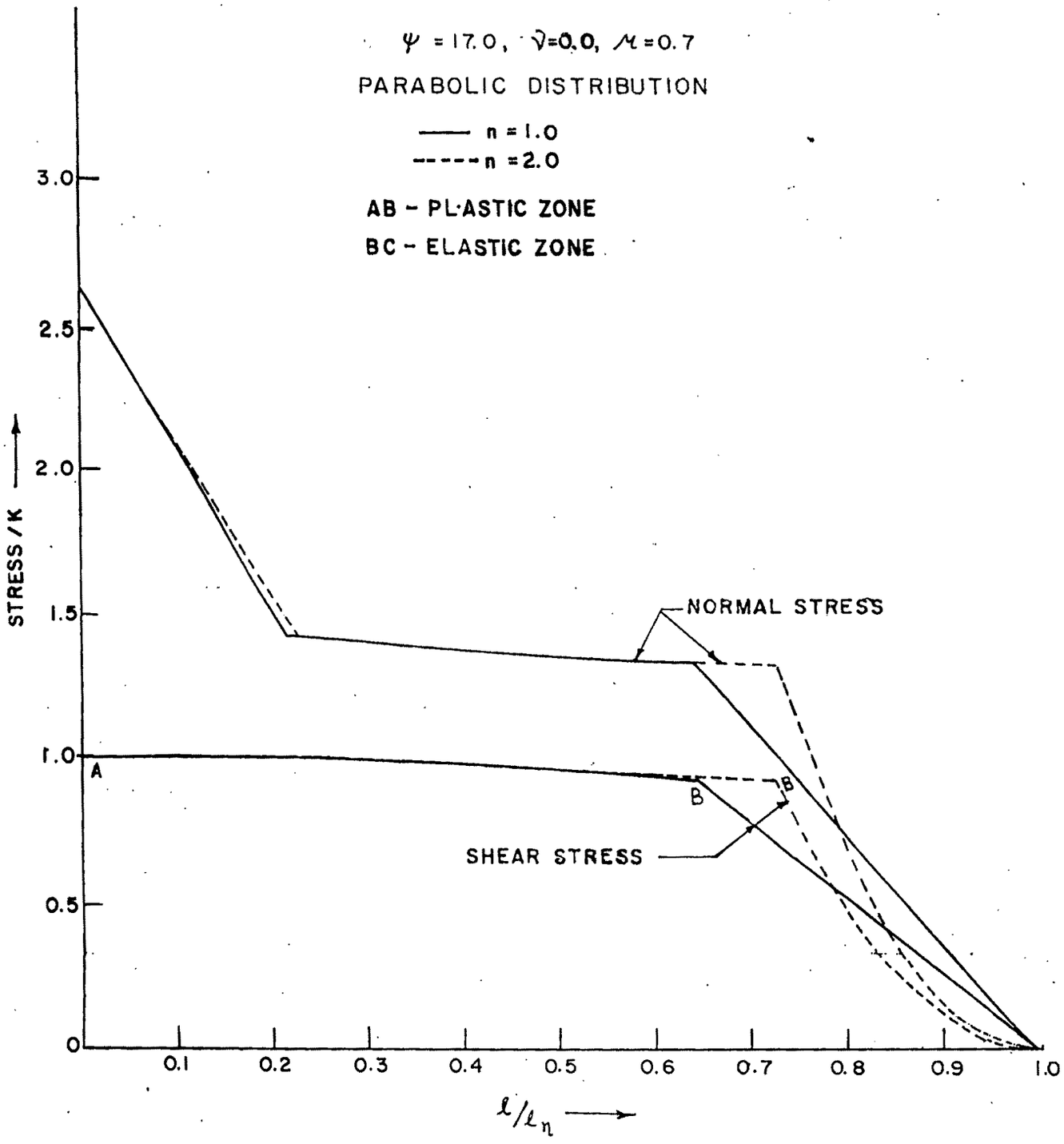

FIG. 5.16 VARIATION OF INTERFACE CONTACT STRESS (SOLUTION-III FIG.5.3)

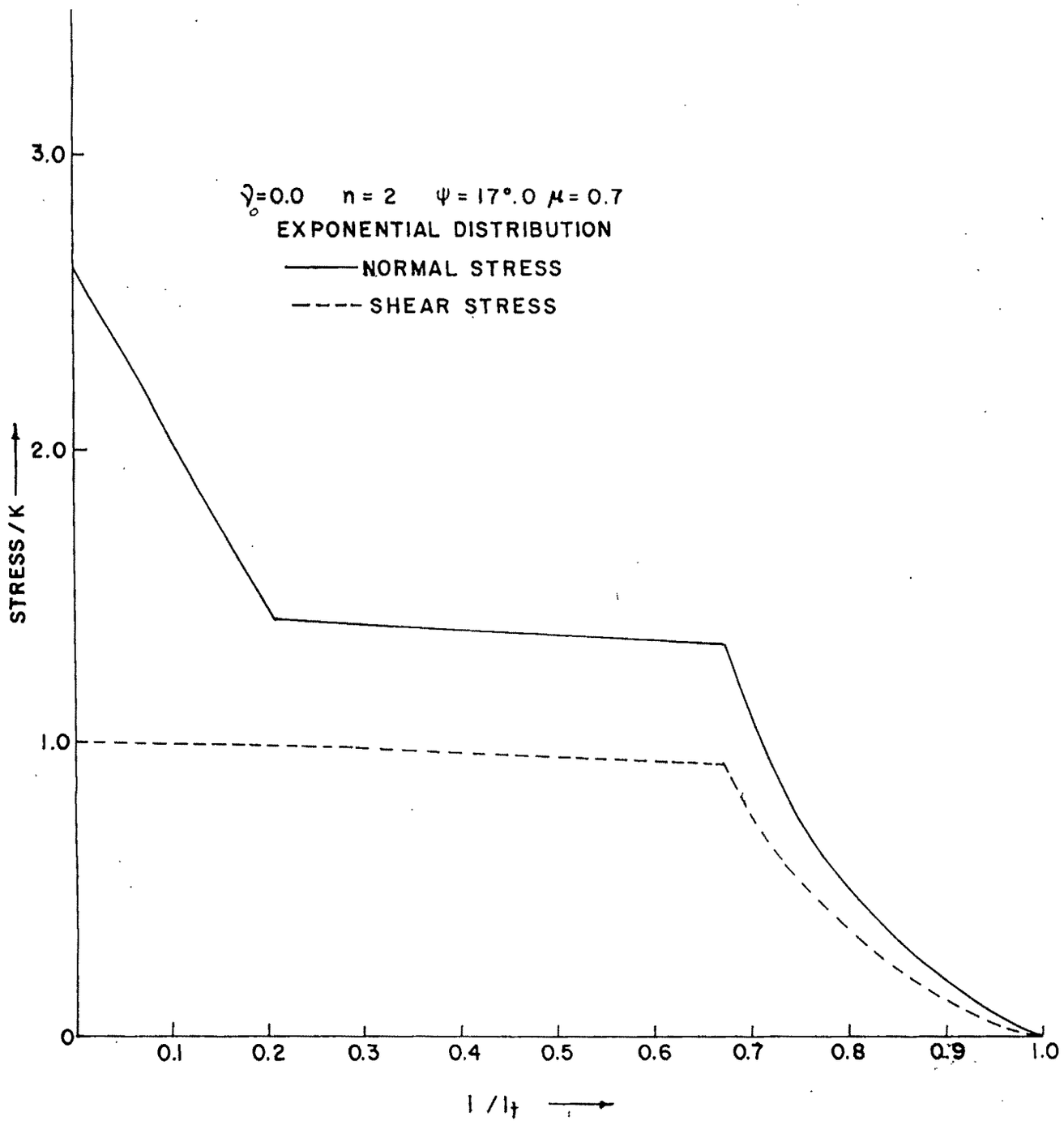

FIG. 5.17 VARIATION OF INTERFACE CONTACT STRESS (SOLUTION-III FIG.5.3)

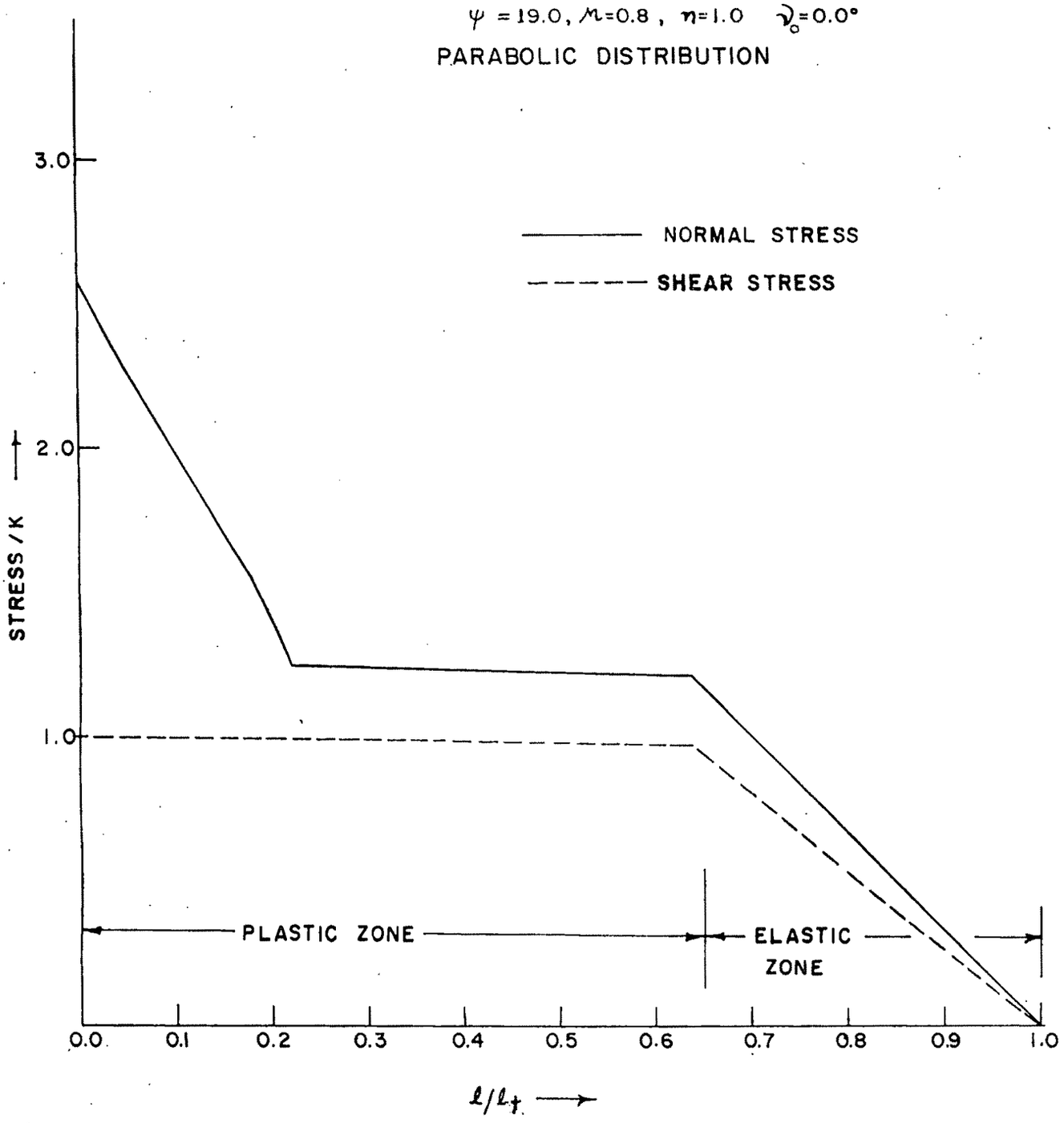

FIG. 5.18 VARIATION OF INTERFACE CONTACT STRESS (SOLUTION-III, FIG. 5.3)

stress distribution in the elastic contact length. Referring to the above figures, it may be seen that for solution II (Fig. 5.2) the normal pressure increases montonically in the region of plastic contact (Fig. 5.13 and Fig. 5.14). For solution III (Fig. 5.3), however, the normal pressure after increasing monotonically in the length of elastic contact, reaches a plateau after which it increases steeply towards the tool tip. The latter observation is in agreement with the experimental results reported by Childs et al.[74] for machining of mild steel. Increasing the value of the exponent "n" (equation 4.5) is found to increase marginally the length of plastic contact (Fig.5.16). The normal pressure at the tool tip, however, is seen to be unaffected by the coefficient of friction μ and the nature of stress distribution in the length of elastic contact. This also agrees with the experimental observations reported by Childs et al.[74].

5.5 Conclusion

1. Two slipline field models with sticking and slipping zones in the length of plastic contact have been developed assuming coulomb friction at the chip-tool interface after modifying the fields suggested by Kudo[34]. The models give both statically as well as kinematically admissible solutions when assumption is made of an elastic zone at the chip-tool interface. The stress-distribution at the chip-tool interface in the sticking and slipping zones have been predicted as a part of the solution.
2. The sticking length and total contact length per unit undeformed chip-thickness increase with increase in co-efficient of friction and decrease with increase in rake angle.

3. The ratio of sticking length to natural contact length is not influenced significantly by change in rake angle. But the above ratio increases with increase in coefficient of friction.
4. The variation of normal and shear stresses in the chip-tool interface as obtained analytically , agrees well with experimental results.

5.6 Plotting of slipline fields

In the subsequent sections , the slipline field network with associated hodographs for some rake angles are presented with similar procedure as discussed in section 3.6. These slipline fields with associated hodographs are shown in figure 5.19 to 5.24. In all cases, the field angles to which the solutions apply are also mentioned.

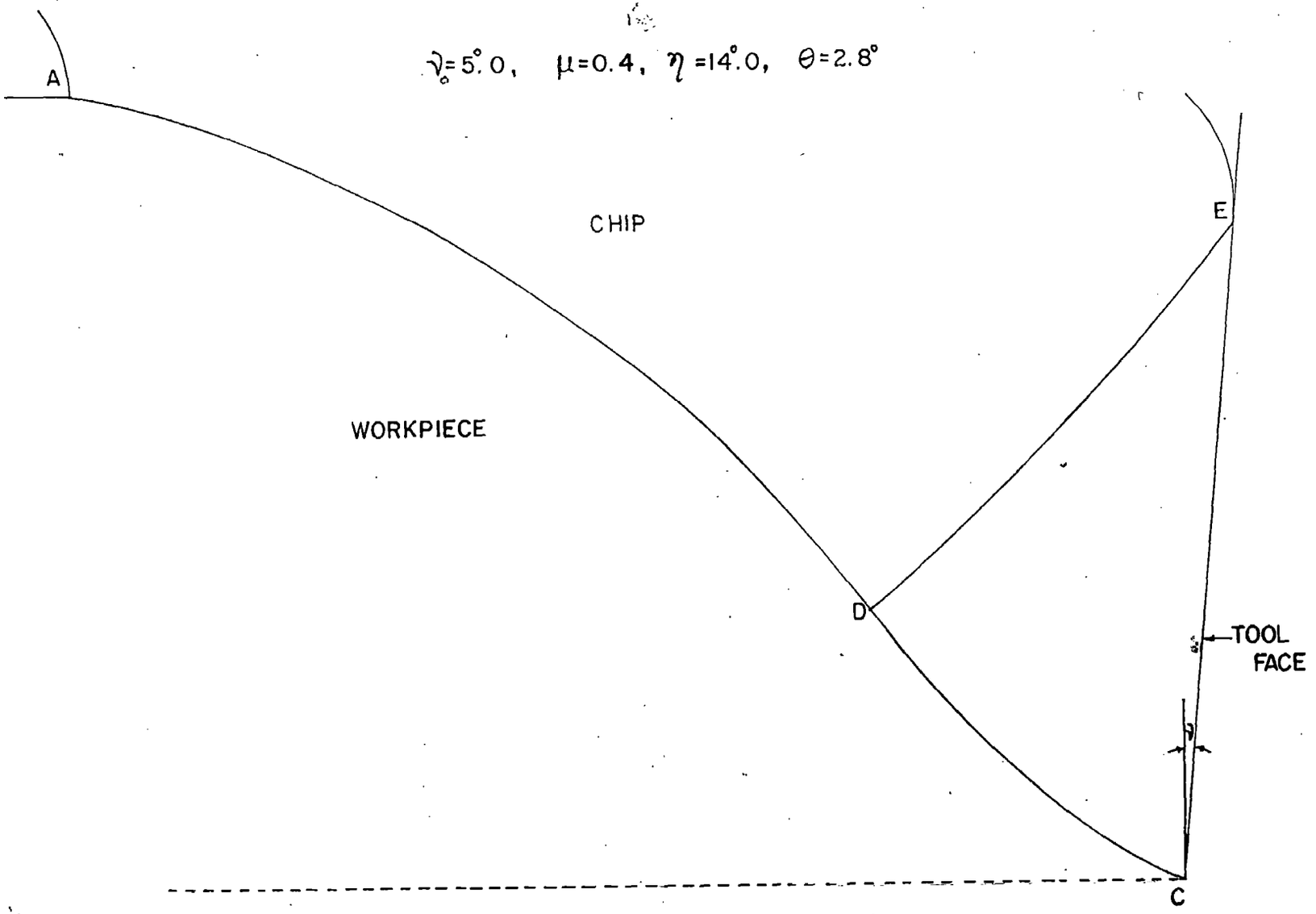

FIG.5.19(a) SLIPLINE FIELD SOLUTION -I (FIG.5.1(a))

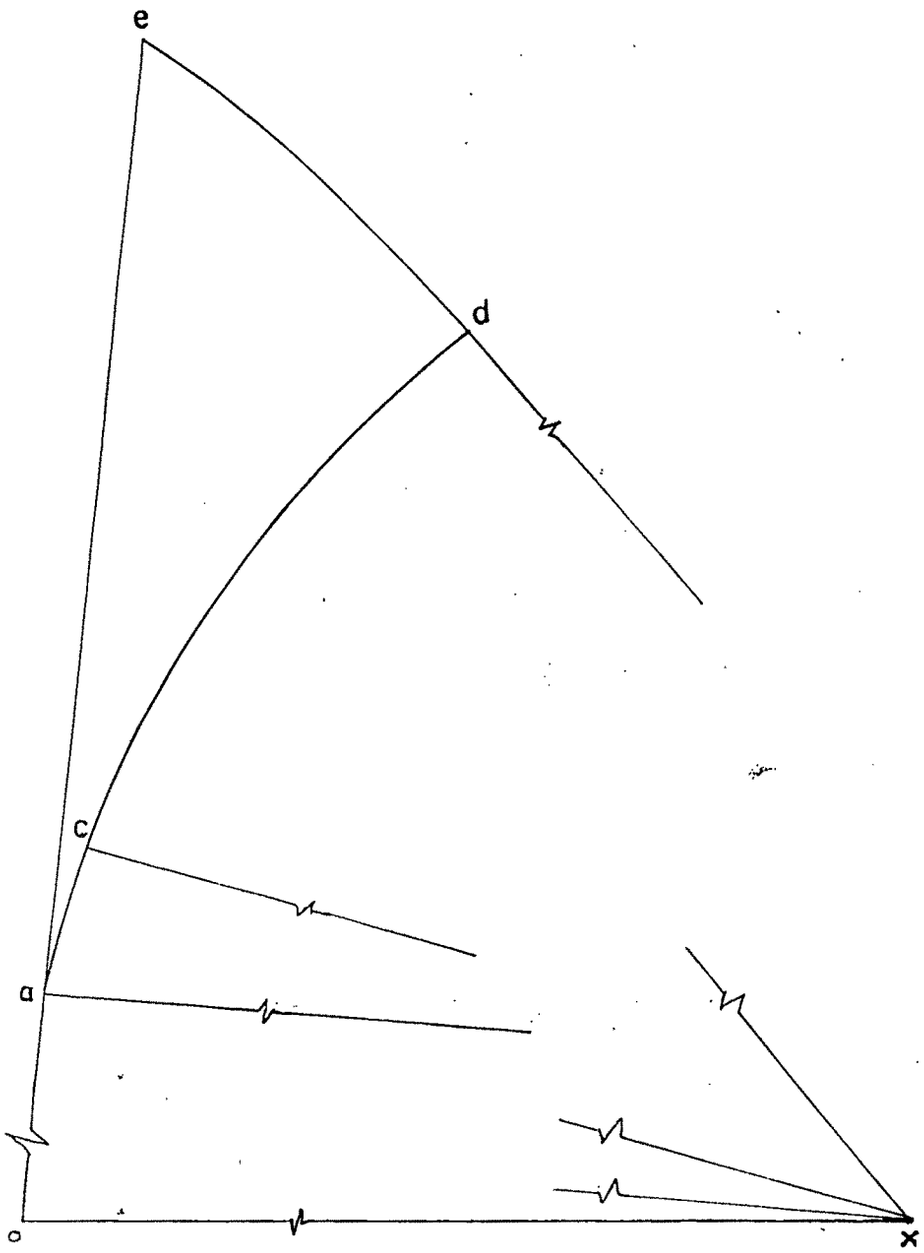

FIG. 5.19(b) HODOGRAPH FOR SLIPLINE FIELD (FIG. 5.19(a))

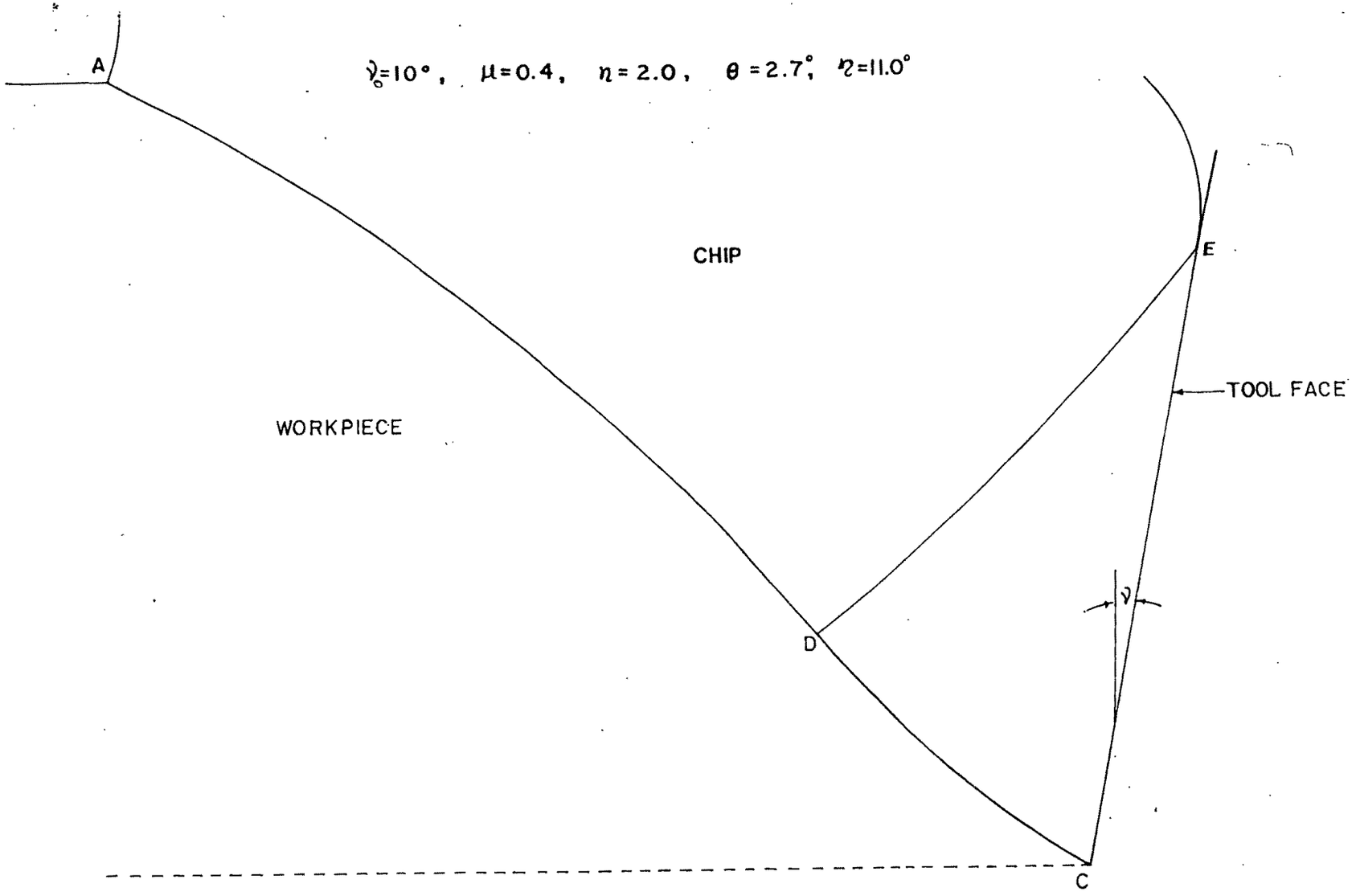

FIG.5.20(a) SLIPLINE FIELD SOLUTION-I (FIG.5.1(a))

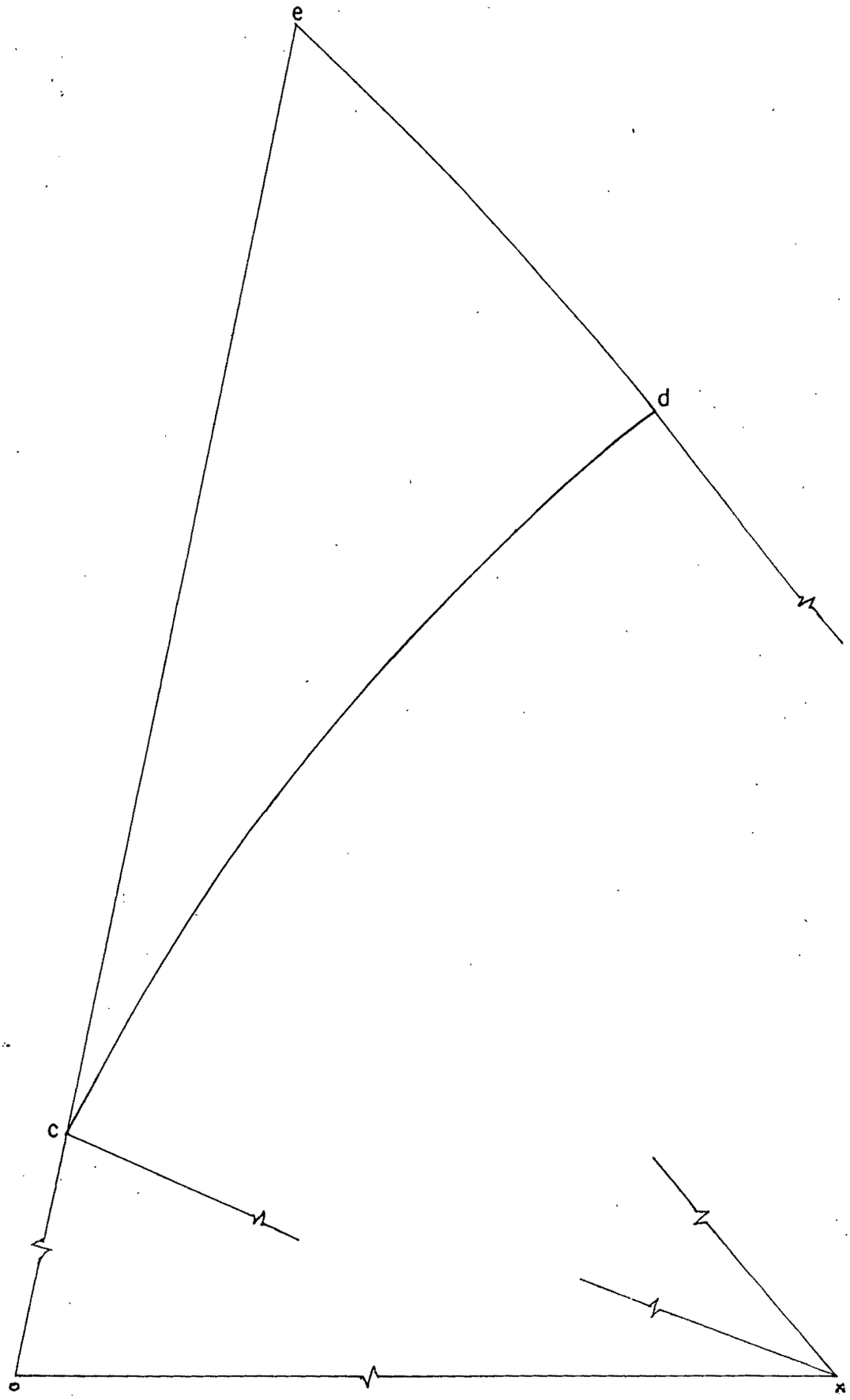

FIG. 5.20(b) HODOGRAPH FOR SLIPLINE FIELD (FIG. 5.20(a))

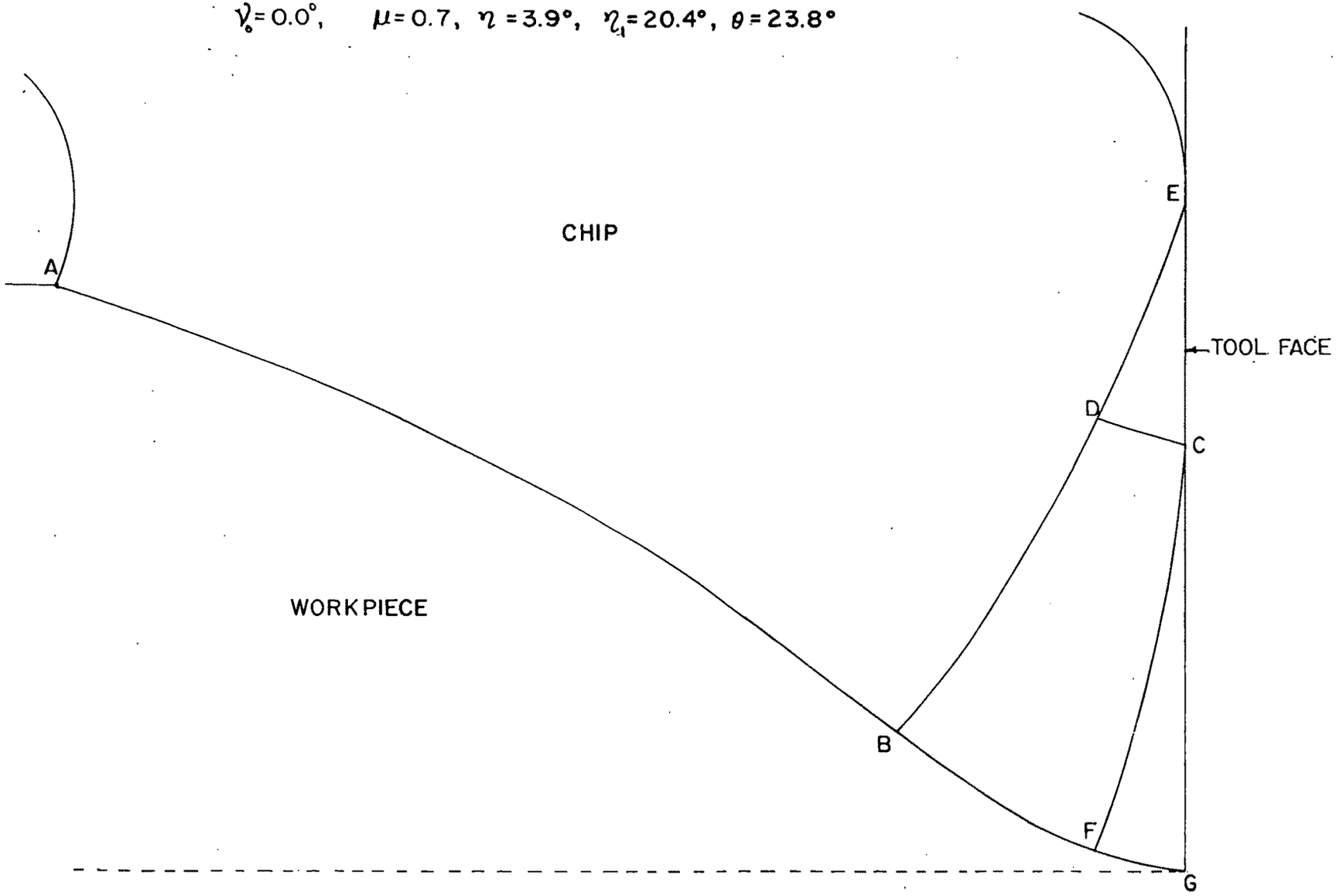

FIG.5.21(a) SLIPLINE FIELD SOLUTION-II (FIG. 5.2(a))

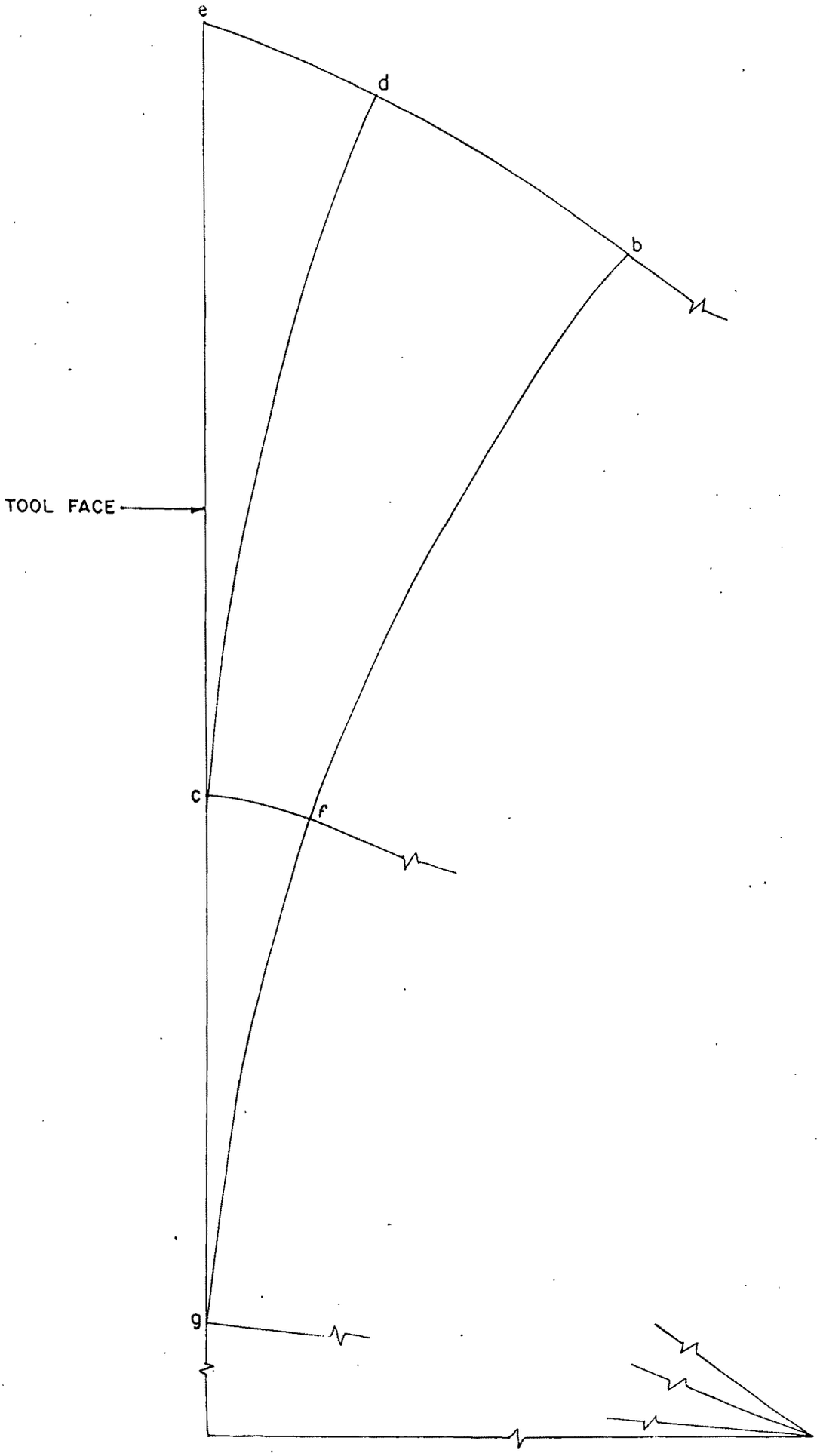

FIG.5.21(b) · HODOGRAPH FOR SLIPLINE FIELD SOLUTION-II (FIG.5.21(a))

$\mu=0.7$, $\gamma_o=10°.0$, $\psi=9°.0$, $\eta=2.4°$, $\eta_1=14.7°$, $\theta=10.4°$

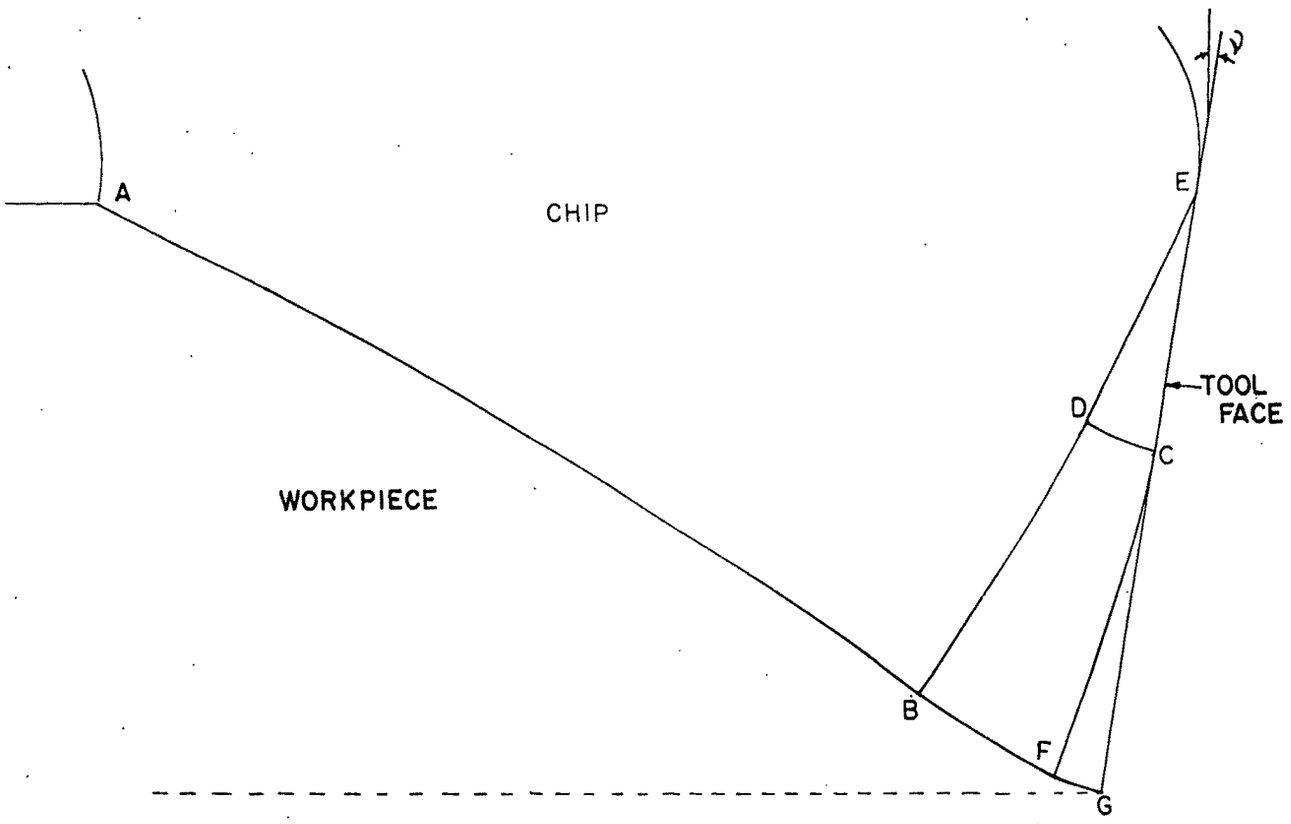

FIG.5.22(a) SLIPLINE FIELD SOLUTION-II (FIG.5.2(a))

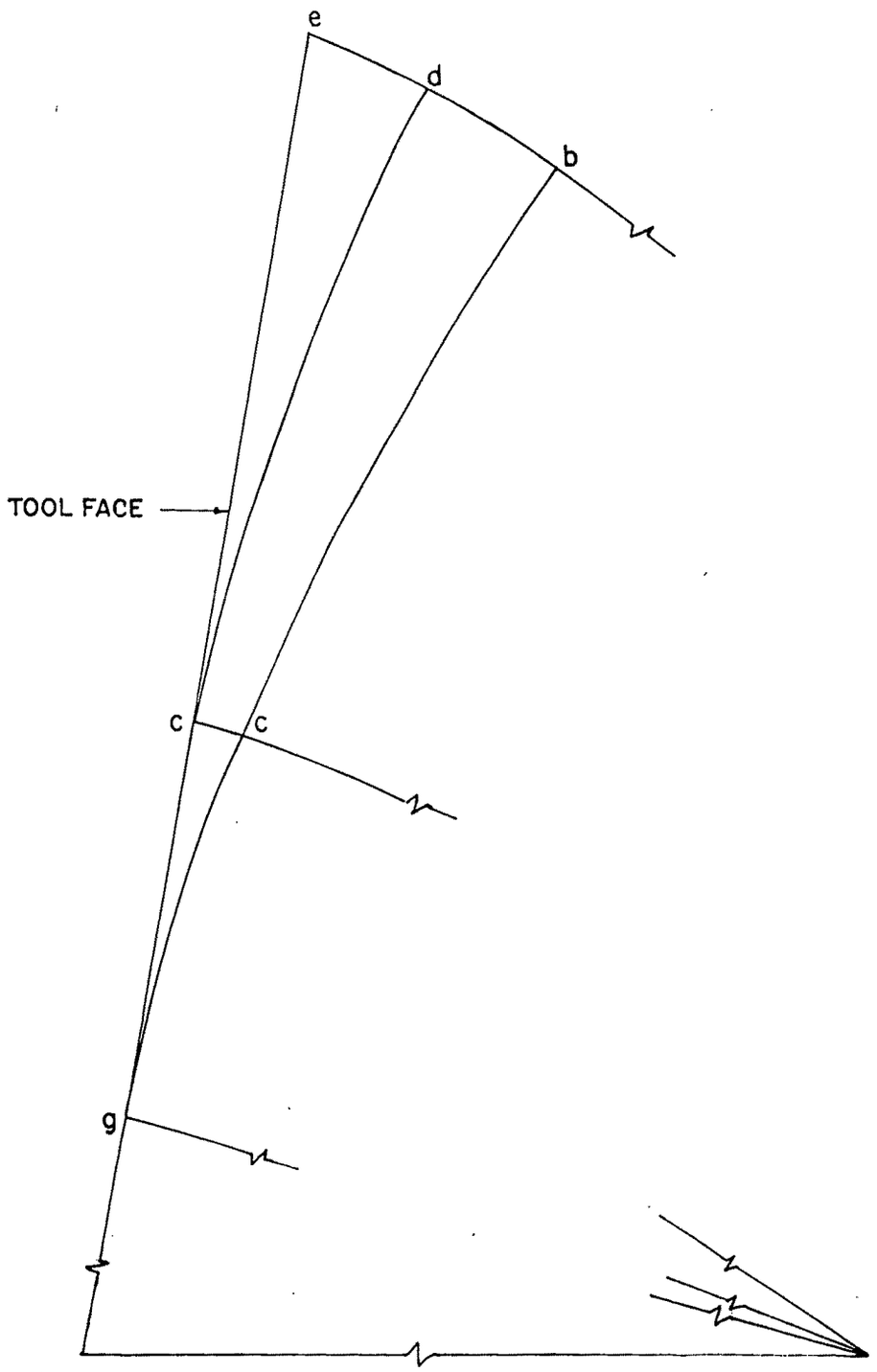

FIG.5.22(b) HODOGRAPH FOR SLIPLINE FIELD (FIG.5.22(a))

$\mu = 0.6$, $\gamma_o = 0.0°$, $\psi = 12°$, $\eta = 32°$, $\eta_1 = 16.5°$, $\theta = 1.05°$

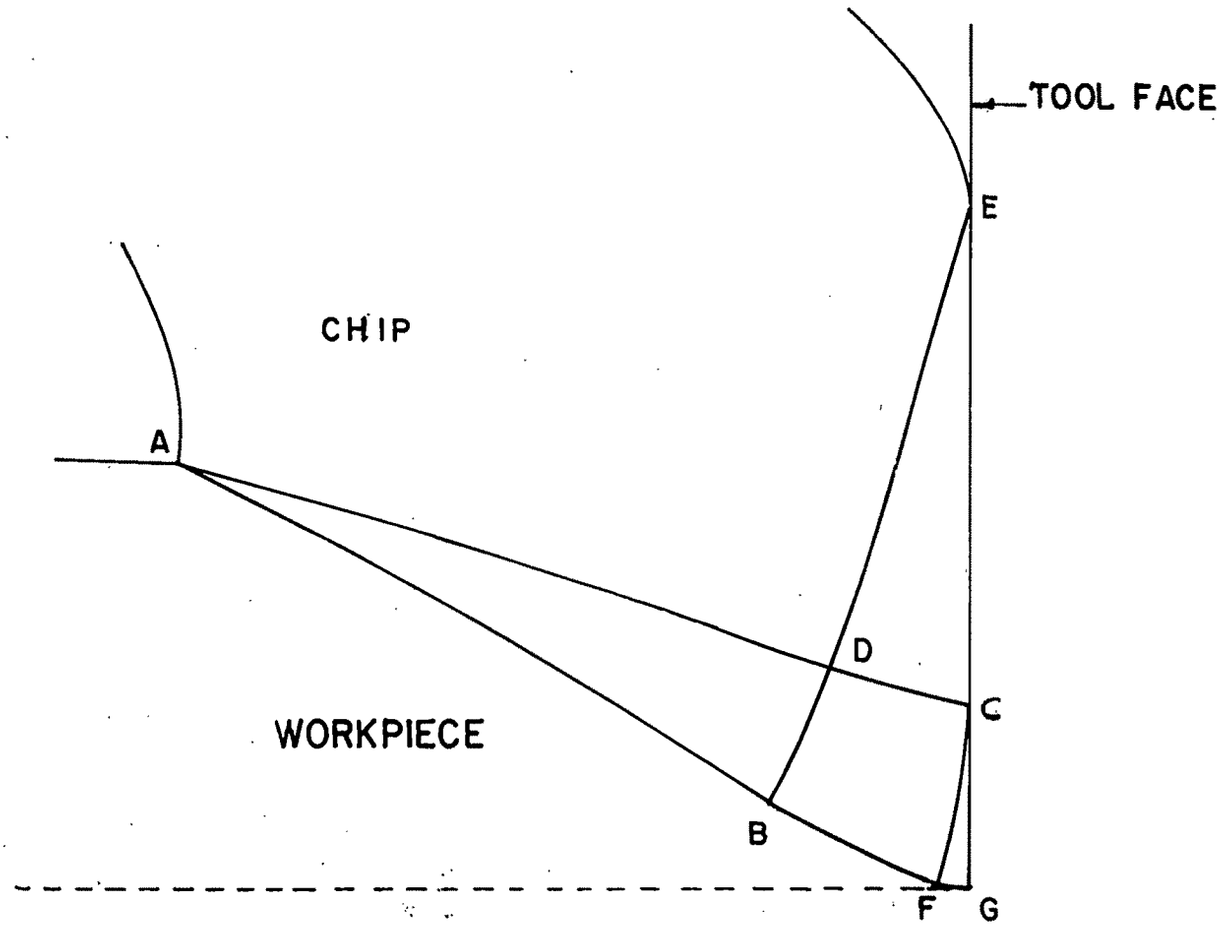

FIG. 5.23(a) SLIPLINE FIELD SOLUTION - III (FIG. 5.3(a))

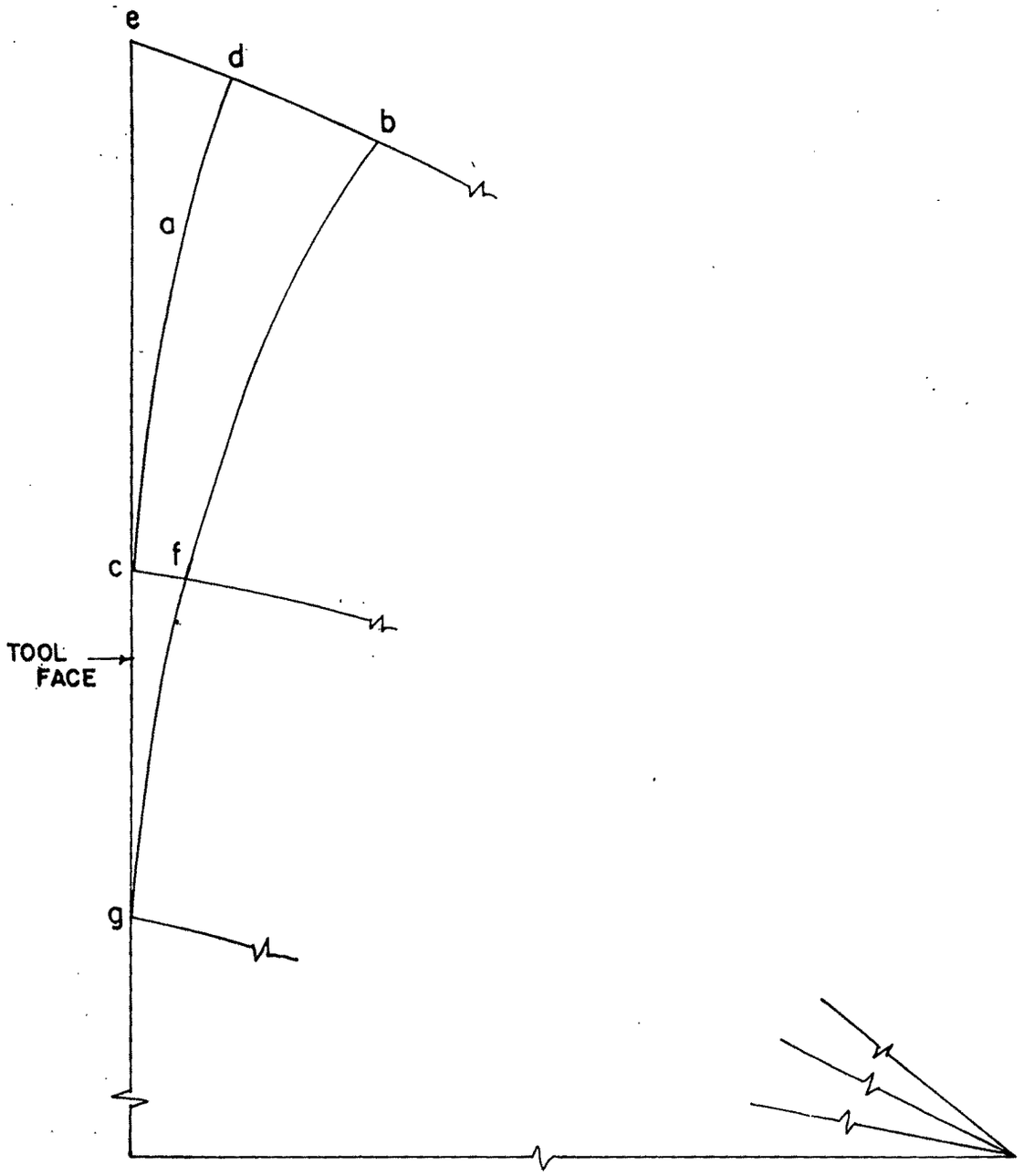

FIG. 5.23(b) HODOGRAPH FOR SLIPLINE FIELD (FIG. 5.23(a))

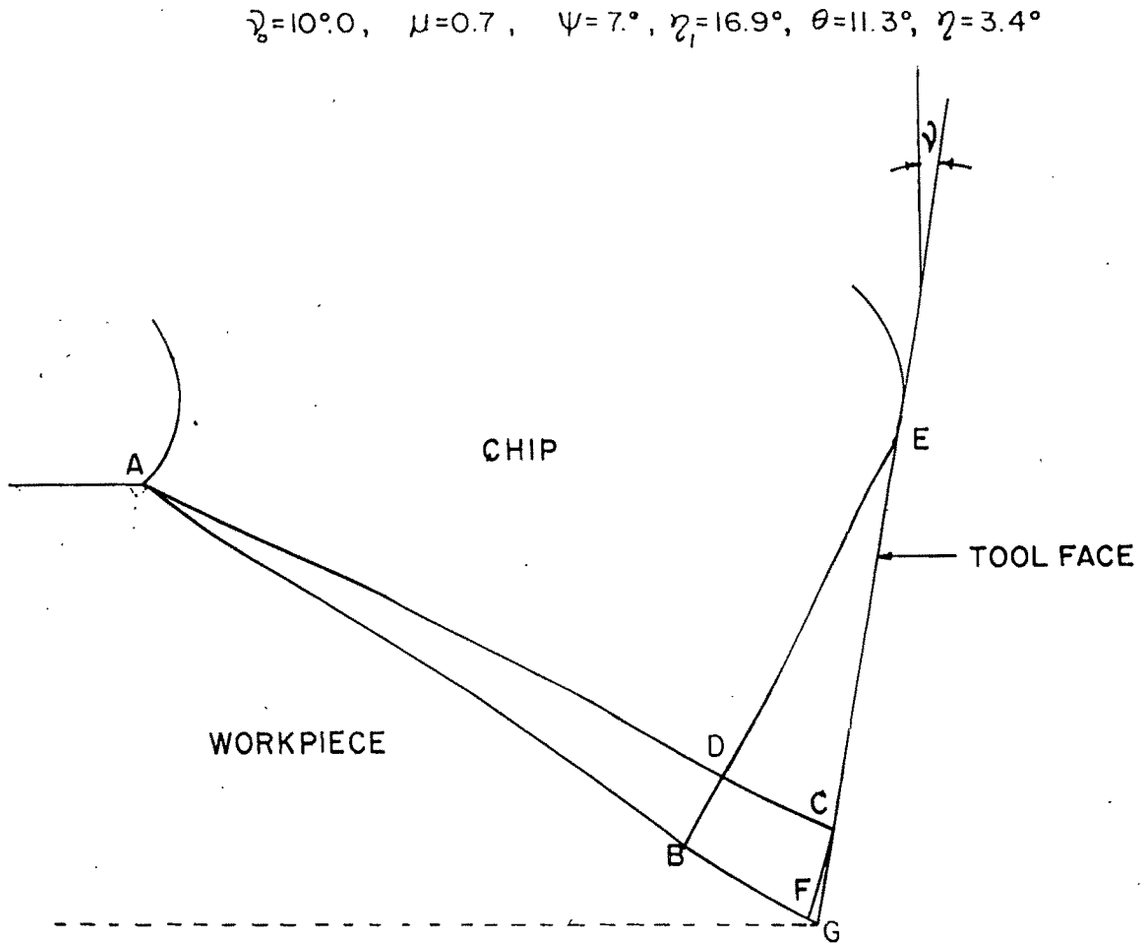

FIG. 5.24(a) SLIPLINE FIELD SOLUTION -III (FIG. 5.3(a)

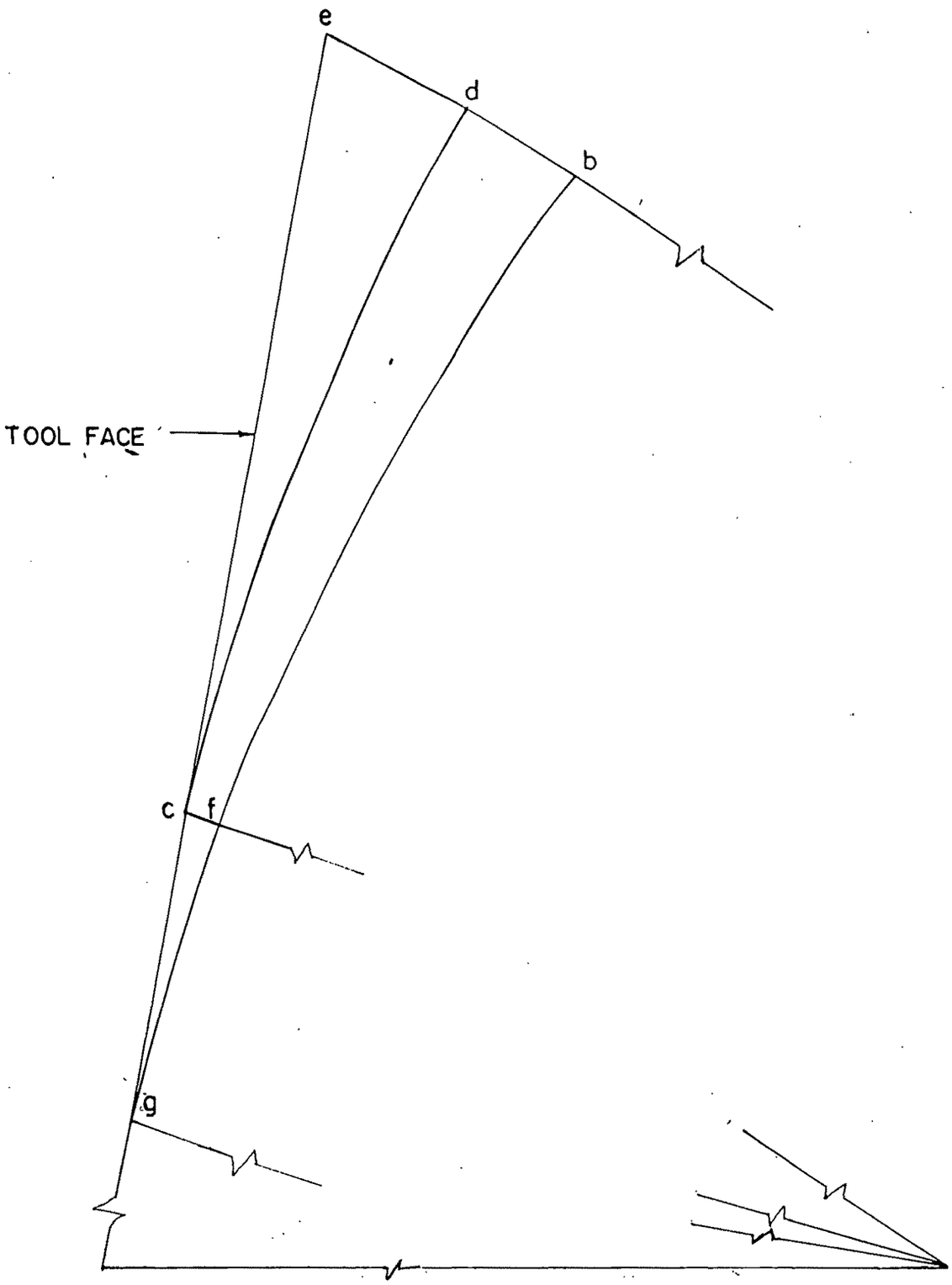

FIG. 5.24(b). HODOGRAPH FOR SLIPLINE FIELD (FIG. 5.24(a))